Enclosure B
Part 2
ST-HL-AE-1617

WCAP 10490

FOR UNRESTRICTED DISTRIBUTION

DATE _____ WNES

TECHNICAL BASES FOR ELIMINATING PRESSURIZER SURGE LINE RUPTURES AS THE STRUCTURAL DESIGN BASIS FOR SOUTH TEXAS PROJECT

Westinghouse Nuclear Energy Systems

WCAP 10490

TECHNICAL BASES FOR ELIMINATING PRESSURIZER SURGE LINE RUPTURES AS THE STRUCTURAL DESIGN BASIS FOR SOUTH TEXAS PROJECT

S. A. Swamy
J. C. Schmertz
A. D. Sane
W. T. Kaiser

February, 1984

APPROVED: J. N. Chirigos

J. N. Chirigos, Manager
Structural Materials
Engineering

APPROVED: E. R. Johnson

E. R. Johnson, Manager
Structural and Seismic
Development

TABLE OF CONTENTS

TABLE OF CONTENTS (Continued)

LIST OF ILLUSTRATIONS

LIST OF ILLUSTRATIONS (Continued)

LIST OF TABLES

1.0 INTRODUCTION

1.1 BACKGROUND

The current structural design basis for the pressurizer surge line requires postulating non mechanistic circumferential (guillotine) breaks in which the pipe is assumed to rupture along the full circumference of the pipe. This results in overly conservative estimates of support loads. It is, therefore, highly desirable to be realistic in the postulation of pipe breaks for the pressurizer surge line. Presented in this report is the description of a mechanistic pipe break evaluation method that can be used for establishing that a guillotine type break will not occur within the pressurizer surge line.

1.2 SCOPE AND OBJECTIVE

The general purpose of this investigation is to show that a circumferential flaw which is larger than any flaw that would be present in the surge line will remain stable when subjected to the worst combination of plant loadings. The flaw stability criteria proposed for the analysis will examine both the global and local stability. The global analysis is carried out using the [ ] method, based on traditional [ ] +a,c,e concepts, but accounting for [ ] and taking into account the +a,c,e presence of a flaw. This analysis enables determination of the critical flaw size. The local stability analysis is carried out by performing a [+a,c,e] of a straight piece of the surge line pipe containing a through-wall circumferential flaw subjected to internal pressure and external loading. This local analysis shows that unstable crack extension will not result for a flaw [ ] +a,c,e calculated by the global analysis.

The leak rate is calculated for the [ ] condition. [+a,c,e] The crack opening area resulting from [ ] loads is determined from an +a,c,e assumed through-wall flaw [ ] +a,c,e [ ] is accounted for in determining the leak rate through this +a,c,e crack. The leak rate is compared with the detection criterion of 1 gpm (Reg. Guide 1.45). The leak rate prediction model is an [+a,c,e

] This method was used [redacted] earlier to estimate the leak rates through postulated cracks in the PWR primary coolant loop.[1-1]

1.3 REFERENCES

1-1 Palusamy, S. S. and Hartmann, A. J., "Mechanistic Fracture Evaluation of Reactor Coolant Pipe Containing a Postulated Circumferential Through-Wall Crack," WCAP-9570, Rev. 2, Class 3, June 1981, Westinghouse Nuclear Energy Systems.

2.0 FAILURE CRITERIA FOR FLAWED PIPES

2.1 GENERAL CONSIDERATIONS

Active research is being carried out in industry, universities as well as other research organizations to establish fracture criteria for ductile materials. Criteria, being investigated, include those based on J integral initiation toughness, equivalent energy, crack opening displacement, crack opening stretch, crack opening angle, net-section yield, tearing modulus and void nucleation. Several of these criteria are discussed in a recent ASTM publication [2-1].

A practical approach based on the ability to obtain material properties and to make calculations using the available tools, was used in selecting the criteria for this investigation. The ultimate objective is to show that the pressurizer surge line containing a conservatively assumed circumferential through-wall flaw is stable under the worst combination of postulated and operating condition loads within acceptable engineering accuracy. With this viewpoint, two mechanisms of failure, namely, local and global failure mechanisms should be considered.

2.2 GLOBAL FAILURE MECHANISM

For a tough ductile material if one assumes that the material is notch insensitive then the global failure will be governed by plastic load. Extensive literature is available on this subject. The recent PVRC study [2-2], reviews the literature as well as data from several tests on piping components, and discusses the details of analytical methods, assumptions and methods of correlating experiments and analysis.

A schematic description of the plastic behavior and the definition of plastic load is shown in Figure 3-1. For a given geometry and loading, the plastic load is defined to be the peak load reached in a generalized load versus displacement plot and corresponds to the point of instability.

A simplified version of this criterion, namely, net section yield criterion has been successfully used in the prediction of the load carrying capacity of pipes containing gross size through-wall flaws [2-3] and was found to correlate well with experiment. This criterion can be summarized by the following relationship:

$$Wa < Wp \qquad (2\text{-}1)$$

where Wa = applied generalized load

Wp = calculated generalized plastic load

In this report, Wp will be obtained by [ ]$^{+a,c,e}$

2.3 LOCAL FAILURE MECHANISM

The local mechanism of failure is primarily dominated by the crack tip behavior in terms of crack-tip blunting, initiation, extension and finally crack instability. The material properties and geometry of the pipe, flaw size, shape and loading are parameters used in the evaluation of local failure.

The stability will be assumed if the crack does not initiate at all. It has been accepted that the initiation toughness, measured in terms of J_{IN} from a J-integral resistance curve is a material parameter defining the crack initiation. If, for a given load, the calculated J-integral value is shown to be less than J_{IN} of the material, then the crack will not initiate.

If the initiation criterion is not met, one can calculate the tearing modulus as defined by the following relation:

$$T_{app} = \frac{dJ}{da}\frac{E}{\sigma_f^2} \qquad (2\text{-}2)$$

where T_{app} = applied tearing modulus

E = modulus of elasticity

σ_f = flow stress = [ ] +a,c,e

a = crack length

[+a,c,e

]

In summary, the local crack stability will be established by the two step criteria:

a,c,e

$$J < J_{IN}, \text{ or} \tag{2-3}$$

$$T_{app} < T_{mat}, \text{ if } J > J_{IN} \tag{2-4}$$

2.4 CORROSION MECHANISM

The Westinghouse reactor coolant system primary loop has an operating history (over 400 reactor years) which demonstrates its inherent stability characteristics. Additionally, there is no history of cracking in RCS primary loop piping. In addition to the fracture resistant materials used in the piping system, the chemistry of the reactor coolant is tightly controlled and variations in temperatures, pressure and flow during normal operating conditions are insignificant.

As stated above, the reactor coolant chemistry is maintained within very specific limits. For example, during normal operation oxygen in the coolant is limited to less than [ ]. This stringent oxygen limit is achieved by +a,c,e controlling charging flow chemistry and maintaning hydrogen in the reactor coolant at a concentration of [ ] The oxygen +a,c,e concentration in the reactor coolant is verified by routine sampling and chemical analysis. Halogen concentrations are also stringently controlled by maintaining concentrations of chlorides and fluorides at or below [ ] +a,c,e This concentration is assured by controlling charging flow chemistry and specifying proper wetted surface materials. Halogen concentrations are also verified by routine chemical sampling and analysis.

2.5 REFERENCES

2-1 J. D. Landes, et al., Editors, Elastic-Plastic Fracture, STP-668, ASTM, Philadelphia, PA 19109, November 1977.

2-2 J. C. Gerdeen, "A Critical Evaluation of Plastic Behavior Data and a Unified Definition of Plastic Loads for Pressure Components," Welding Research Council Bulletin No. 254.

2-3 Mechanical Fracture Predictions for Sensitized Stainless Steel Piping with Circumferential Cracks, EPRI-NP-192, September 1976.

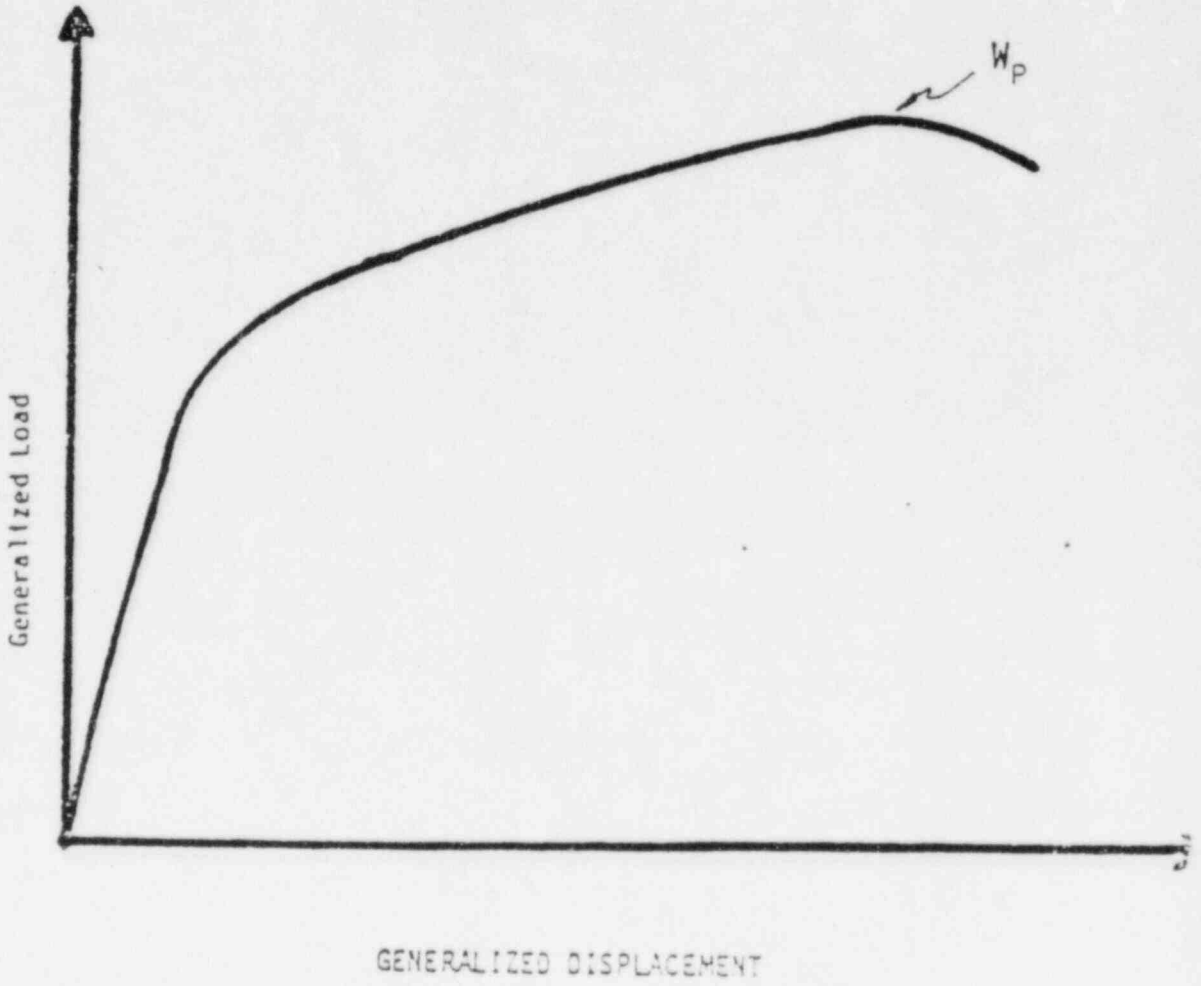

FIGURE 2-1 Typical Load - Deformation Behavior

3.0 LOADS FOR CRACK STABILITY ANALYSIS

The surge line stress report[3-1] was reviewed to identify locations with high ASME NB 3600 faulted (Eq. 9) stresses. These locations are identified on the surge line computer model in Figure 3-1. The loads at each of these locations were tabulated from the computer runs of [3-1] for the [ ] loading cases. +a,c,e

The axial load, bending moment and stress at these locations were calculated from the tabulated loads as follows:

$$F = [\quad] \qquad (3.1) \qquad +a,c,e$$

$$M_Y = [\quad] \qquad (3.2) \qquad +a,c,e$$

$$M_Z = [\quad] \qquad (3.3) \qquad +a,c,e$$

$$M = \sqrt{M_y^2 + M_z^2} \qquad (3.4)$$

$$\sigma = \frac{F}{A} + \frac{M}{Z} \qquad (3.5)$$

where,

subscript [ ] indicate the loading cases, +a,c,e

F_p = axial load due to normal operating pressure
M_y = Y component of moment
M_z = Z component of moment
F = total axial load at the location
M = bending moment at the location
A = metal cross-sectional area of piping
Z = sectional modulus of the pipe

The wrought piping material is the same, [ ] for the entire surge line and hence the location with the highest stress calculated by equation (3.5) was identified as the worst location for the global and the local crack stability analysis of Section 4.0, 5.0, respectively. The [ ] was selected as the critical section based on this criteria (see Table 3-1). The calculated axial load, bending moment and longitudinal stress at this location are: +a,c,e +a,c,e

Type of Analysis	F (K)	M (Ft. K)	σ (ksi)
Global Crack Stability	[		]
Local Crack Stability			

The thermal expansion loading case (TH) used in calculating the loads and stress for the local crack stability analysis corresponds to the normal operating temperature of 653°F. However, the design thermal case with 683°F temperture was conservatively used for the global crack stability analysis.

The operating transients of the surge line are such that no [ ] can occur. +a,c,e

REFERENCES

3-1 EDS report NO. 01-0420-1009, Revision 0, "ASME Boiler and Pressure Vessel Code Section III Class 1 Stress Report for the RCS Pressurizer Surge Line."

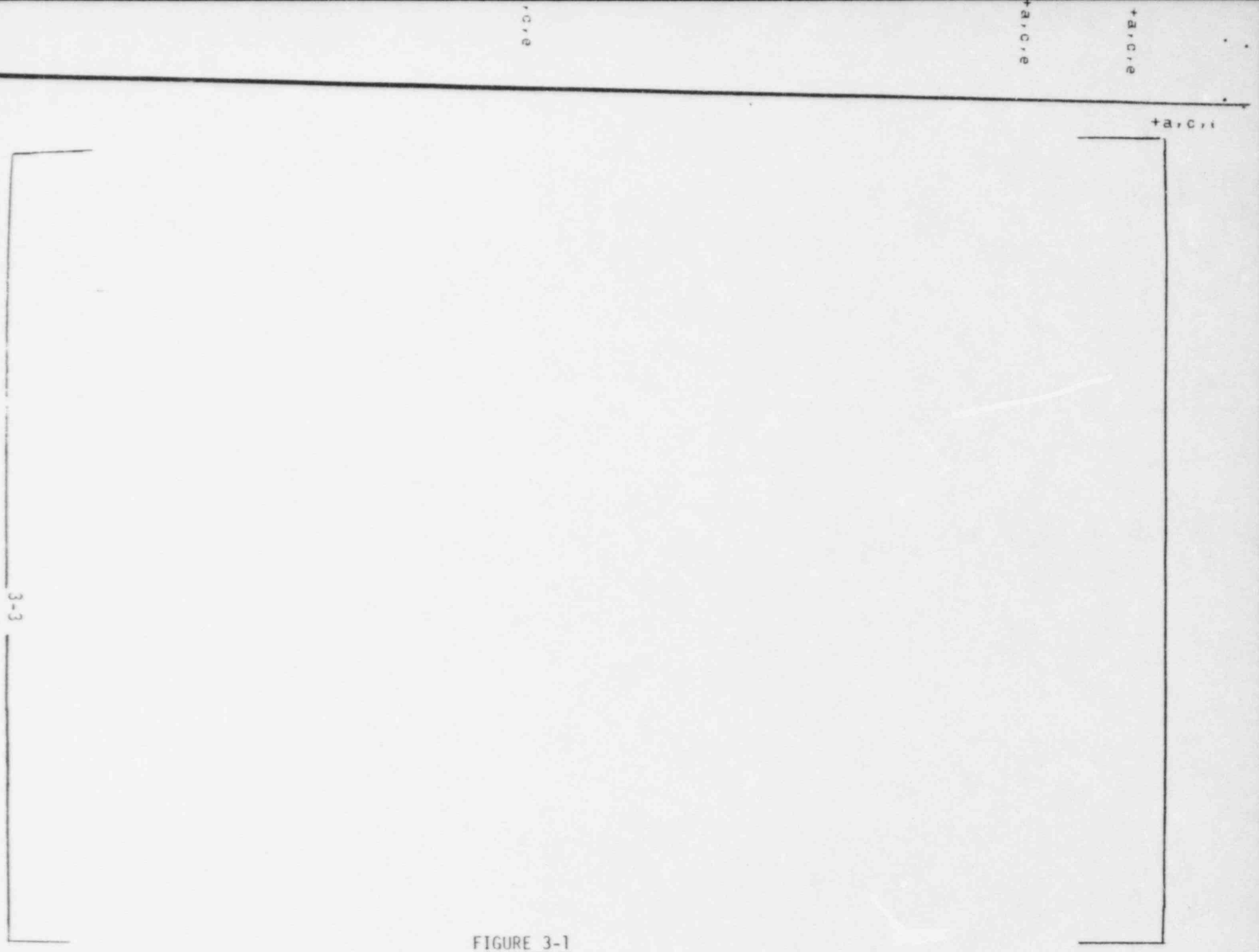

FIGURE 3-1

PRESSURIZER SURGE LINE PIPING ANALYSIS MODEL

TABLE 3-1

A SUMMARY OF SURGE LINE LOCATIONS WITH HIGH LOADS AND STRESSES

Node No.	Axial Force (k)	Bending Moment (ft.-k)	Stress σ (Ksi)
[			+a,c,e]
NOTE: [		+a,c,e]	

4.0 CRITICAL FLAW SIZE CALCULATION

The conditions which lead to failure in stainless steel must be determined using plastic fracture methodology because of the large amount of deformation accompanying fracture. A conservative method for predicting the failure of ductile material is the [+a,c,e

]

The flawed pipe is predicted to fail when [+a,c,e

c,e

] This methodology has been shown to be applicable to ductile piping through a large number of experiments, and will be used here to predict the critical flaw size in the pressurizer surge line. The failure criterion has been obtained by [+a,c,e

] The detailed development is provided in Appendix A, for a through-wall circumferential flaw in a pipe with [

] The [ ] for these conditions is: +a,c,e

+a,c,e

[

(4-1)]

+a,c,e

[ ]

The analytical model described above accurately accounts for the piping internal pressure as well as imposed axial force as they affect the [ ] In order to validate the model, analytical predictions were compare with the experimental results [4-1] as shown in Figure 4.2. Good agreement was found.

In order to calculate the critical flaw size, a plot of the [ ] versus crack length is generated as shown in Figure 4-3. The critical flaw size corresponds to the intersection of this curve and the maximum load line.

The critical flaw size is [ ] using ASME Code[4-2] [ ] stainless steel.

Since W_p[ ] for cracks smaller than [ ] and W_a = [ ] the global stability criterion of Section 2.0 is satisfied. +a

REFERENCE

4-1 Kanninen, M. F., et al., "Mechanical Fracture Predictions for Sensitized Stainless Steel Piping with Circumferential Cracks," EPRI NP-192, September 1976.

4-2 ASME Section III, Division 1-Appendices, 1983 Edition, July 1, 1983.

(4-2)

+a,c,e

ed

+a,c,e

+a,c,e

+a,c,e

+a,c,e

+a,c,e

+a,c,e

+a,c,e

+a,c,e

Figure 4-1 [ ] Stress Distribution

+a,

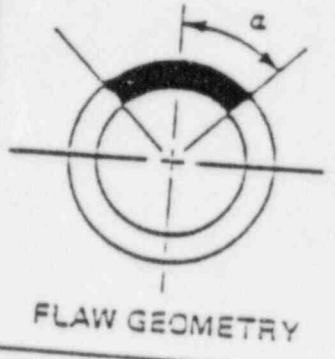

Figure 4-2 Comparison of [ ] predictions with Experimental results +a,c,e

+a,c

PRESSURIZER SURGE LINE USING ASME CODE MINIMUM PROPERTIES

+a,c

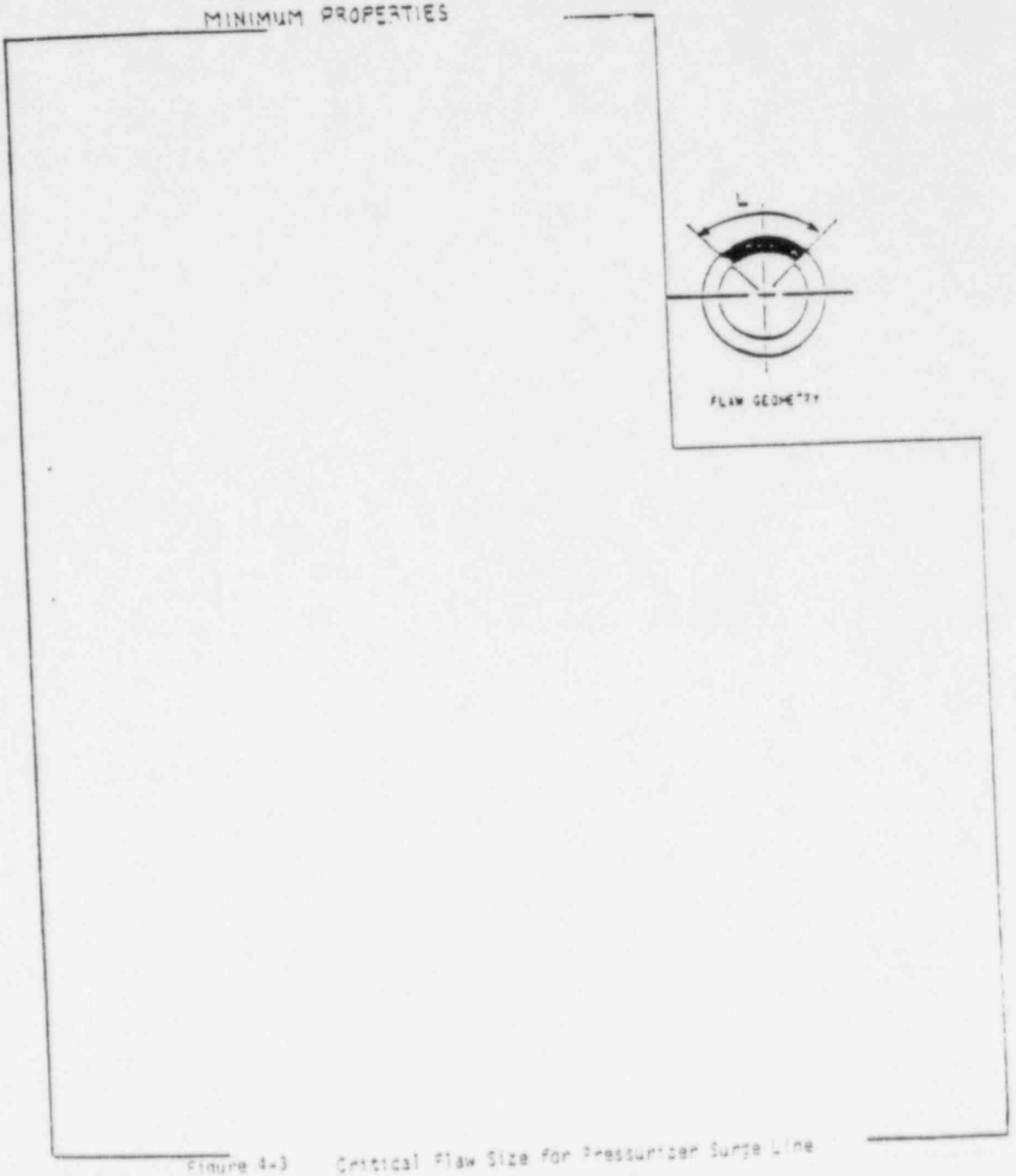

Figure 4-3 Critical Flaw Size for Pressurizer Surge Line

+a,c,e

+a,c

PRESSURIZER SURGE LINE USING ASME CODE MINIMUM PROPERTIES

+a,c

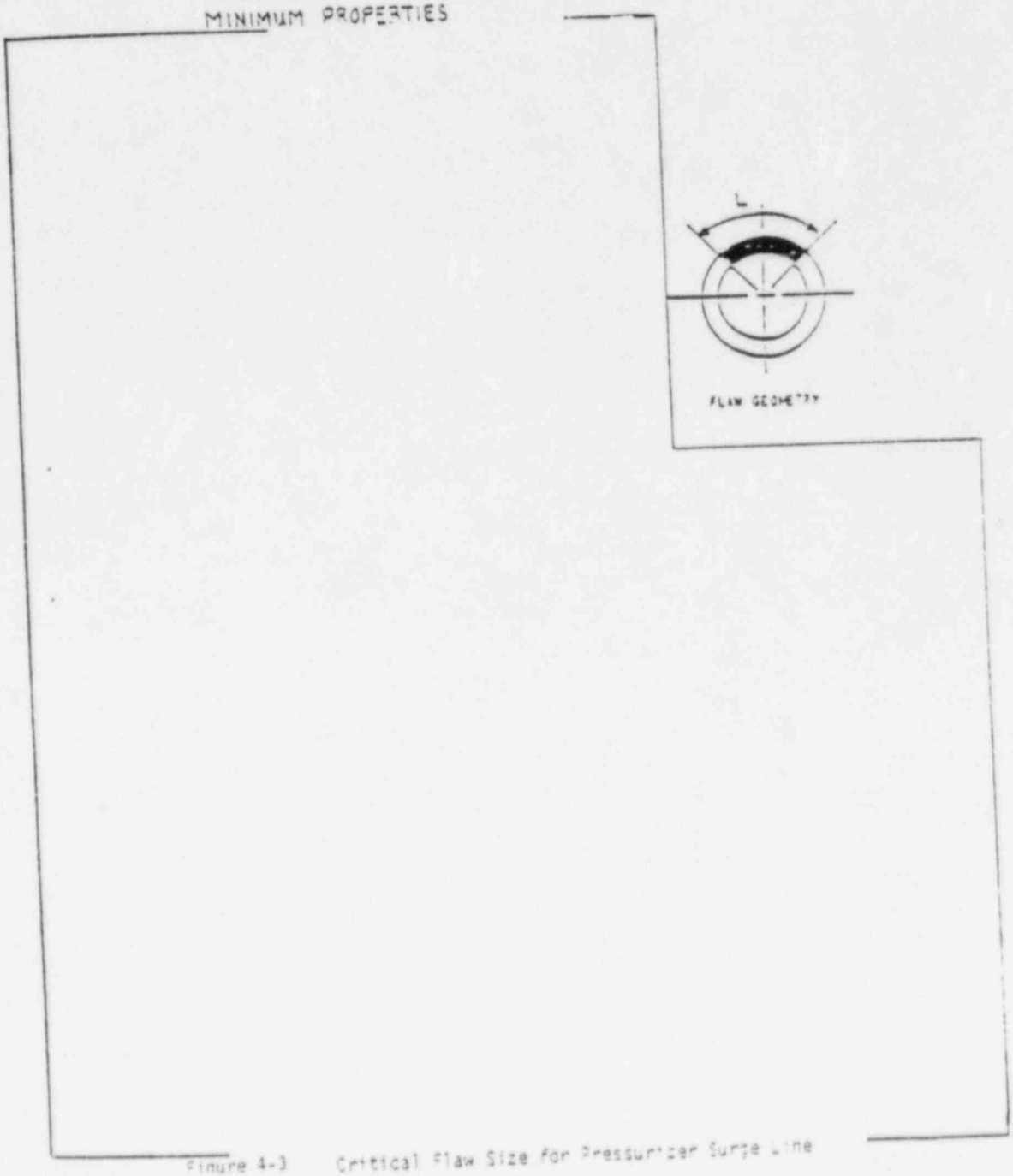

Figure 4-3 Critical Flaw Size for Pressurizer Surge Line

+a,c,e

5.0 [ ] ANALYSIS FOR CRACK STABILITY CALCULATIONS +a,c,e

Using the [ ] computer program, a [ ] crack was analyzed for local instability. The loadings consist of [ ] +a,c,e

5.1 DESCRIPTION OF THE MODEL

Figure 5-1 identifies all the loads acting on the pipe. Figures 5-2 through 5-7 all show the [ ] used for the analysis. [ ] are identified on Figures 5-2 through 5-5. [ ] of interest for later leak rate predictions are shown in detail on Figure 5-7. +a,c,e

+a,c,e

[ ]

5.2 LOADING THE MODEL

Figures 5-8, 5-9, and 5-10 show the sequence of applying the loads to the [ ] of the pipe. Figure 5-8 shows how the pressure of the fluid is applied gradually to the inside wall of the pipe until load step 3, after which it is held steady. As shown in Figure 5-9, the [ ] is also applied gradually. Figure 5-10 shows application of the [ ] starting at load step 3, where the [ ] has reached its full value. +a,c,e

5.3 ELASTO-PLASTIC ANALYSIS

[+a,c,e]

[ ] +a,c,e

5.4 [ ] RESULTS +a,c,e

One sufficient condition for establishing the stability of a crack is that the maximum value of the J integral be less than the initiation toughness J_{IN}. Figure 5-12 shows how the calculated value of the J integral increases up to and beyond the maximum operating loading at [ ] At the maximum loading, +a,c,e
the J integral has a corresponding value of [ ] as shown on +a,c,e
the figure. Since the minimum initiation toughness [+a,c,e
] is larger, the condition for crack stability is fulfilled.
The above value for J_{IN} is obtained from [+a,c,e
]

5.5 VERIFICATION OF [ ] ANALYSIS +a,c,e

For small loadings, the [ ] results for the stress intensity factor (K_I) +a,c,e
should agree with hand calculations developed for Linear Elastic Fracture Mechanics (LEFM). When the loads are large enough for significant elasto-plastic behavior to occur, the [ ] results for the stress intensity +a,c,e
factor should be larger than the hand calculated (LEFM) results.

Figure 5-13, and Table 5-1 show that the relation between the [ ] values +a,c,e
and the LEFM values is as described above.

The LEFM calculations for the stress intensity factor are performed using the method described in [+a,c,e

] (5-1)

+a,c,e

+a,c,e

the

o

y, +a,c,e

on +a,c,e

+a,c,e

+a,c,e

+a,c,e

+a,c,e

y +a,c,e

+a,c,e

+a,c,e

+a,c,e

+a

+a,c,e

+a,c,e

[+a,c,

]

From Table 5-1, the [
compares with [ ] within an accuracy of less than 1 percent.] which +a,c,
+a,c,

5.6 REFERENCES

5-1 [+a,c,e

]

5-2 [+a,c,e

5-3

5 4

]

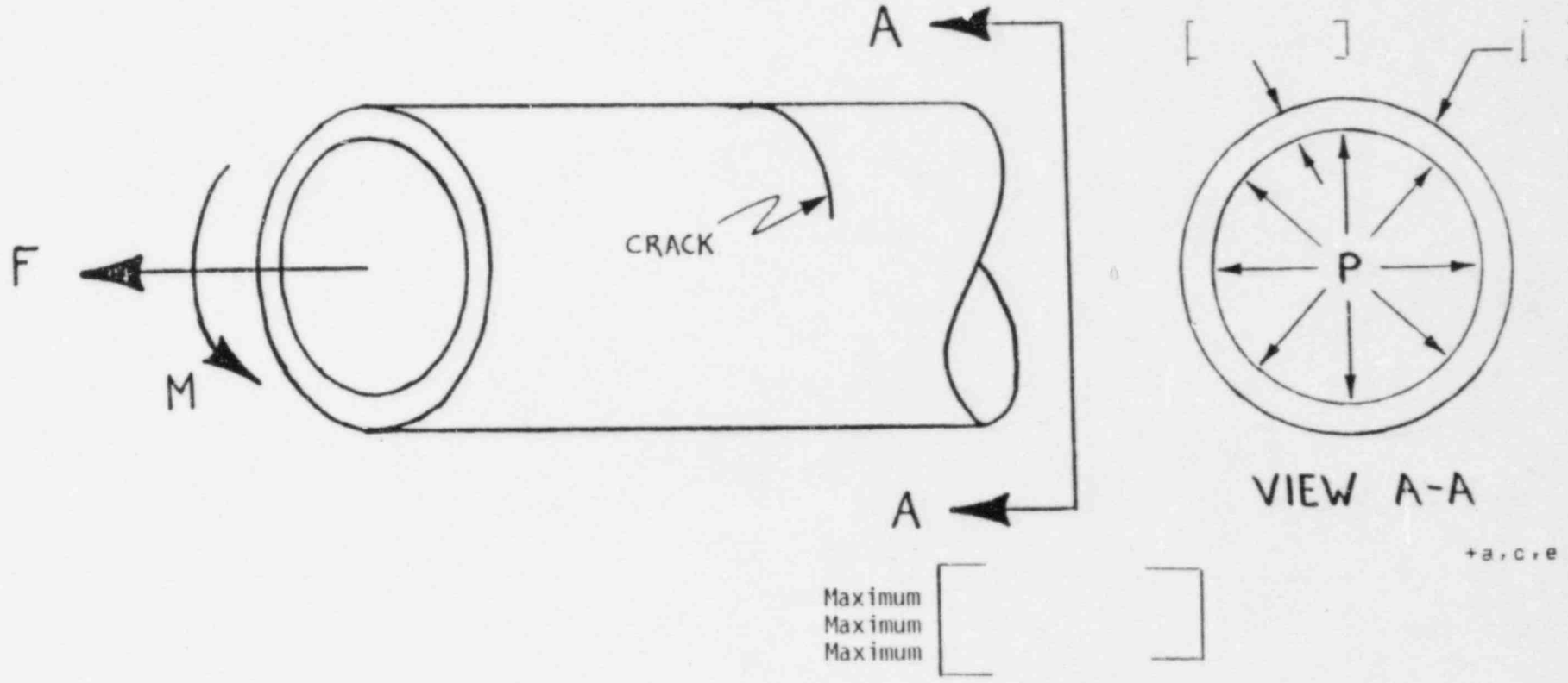

FIGURE 5-1 PIPE LOADING

+a

Fig. 5-2 [ ]Model Geometry with [ ]Circumferential Cra

+a,c,

+a,c,e

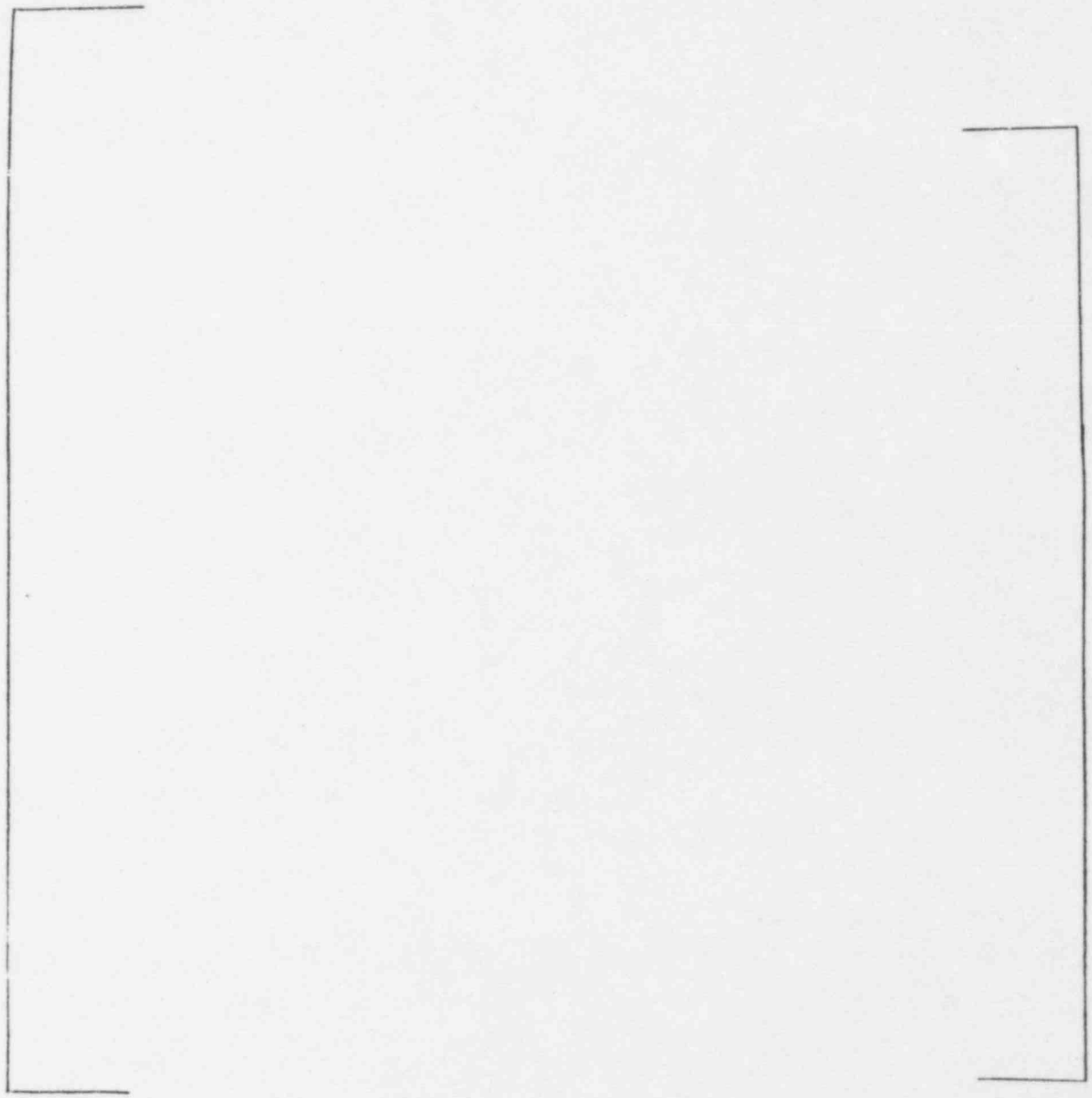

Fig. 5-3 [ ]Model Geometry with [ ]Circumferential Crack -[ ] +a,c,e

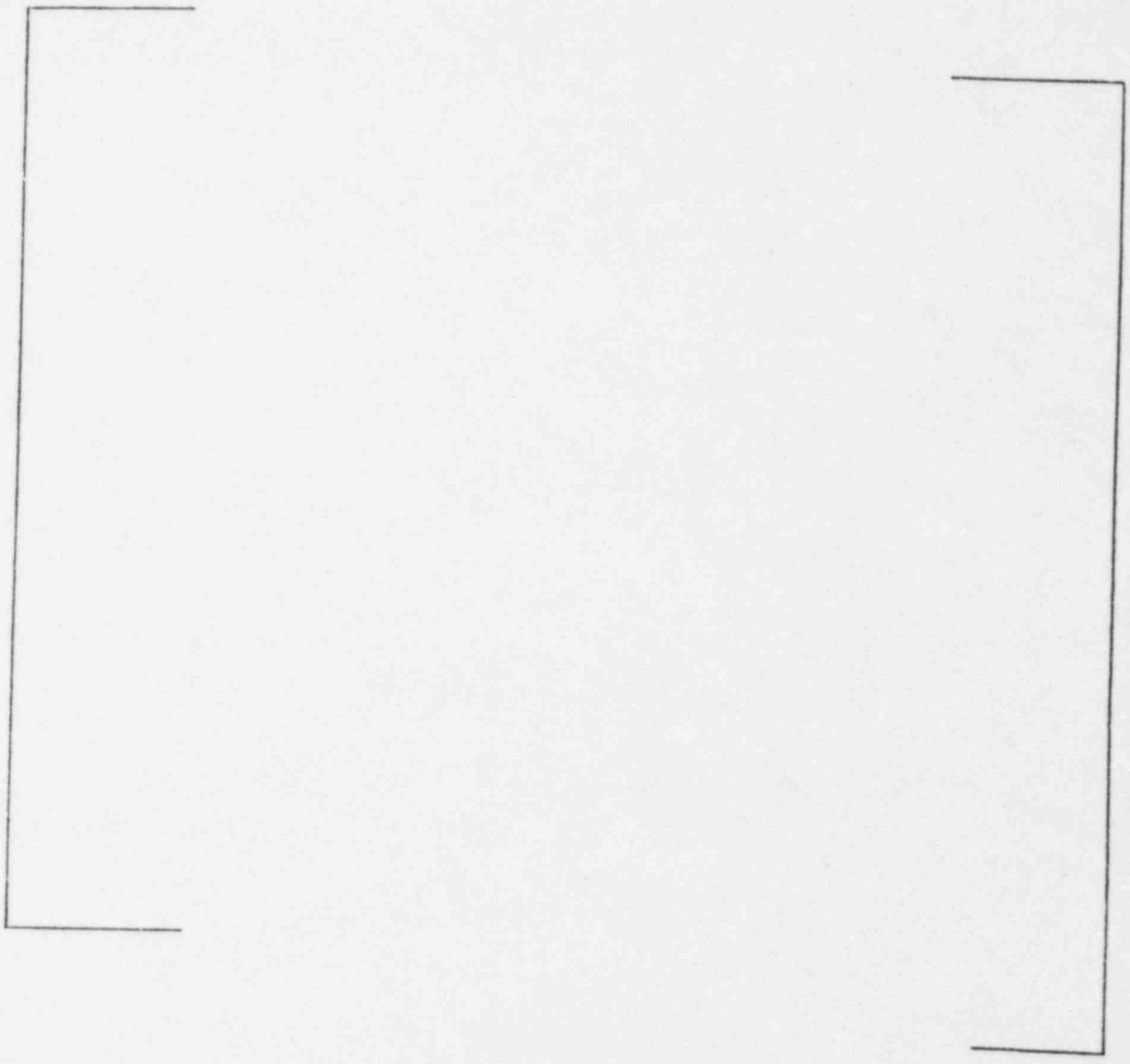

+a,c,e

Fig. 5-4 [ ]Model Geometry with [ ]Circumferential Crack -[ ] +a,c,e

]Model Geometry with[ ]Circumferential Crack -[ ] +a,c,e

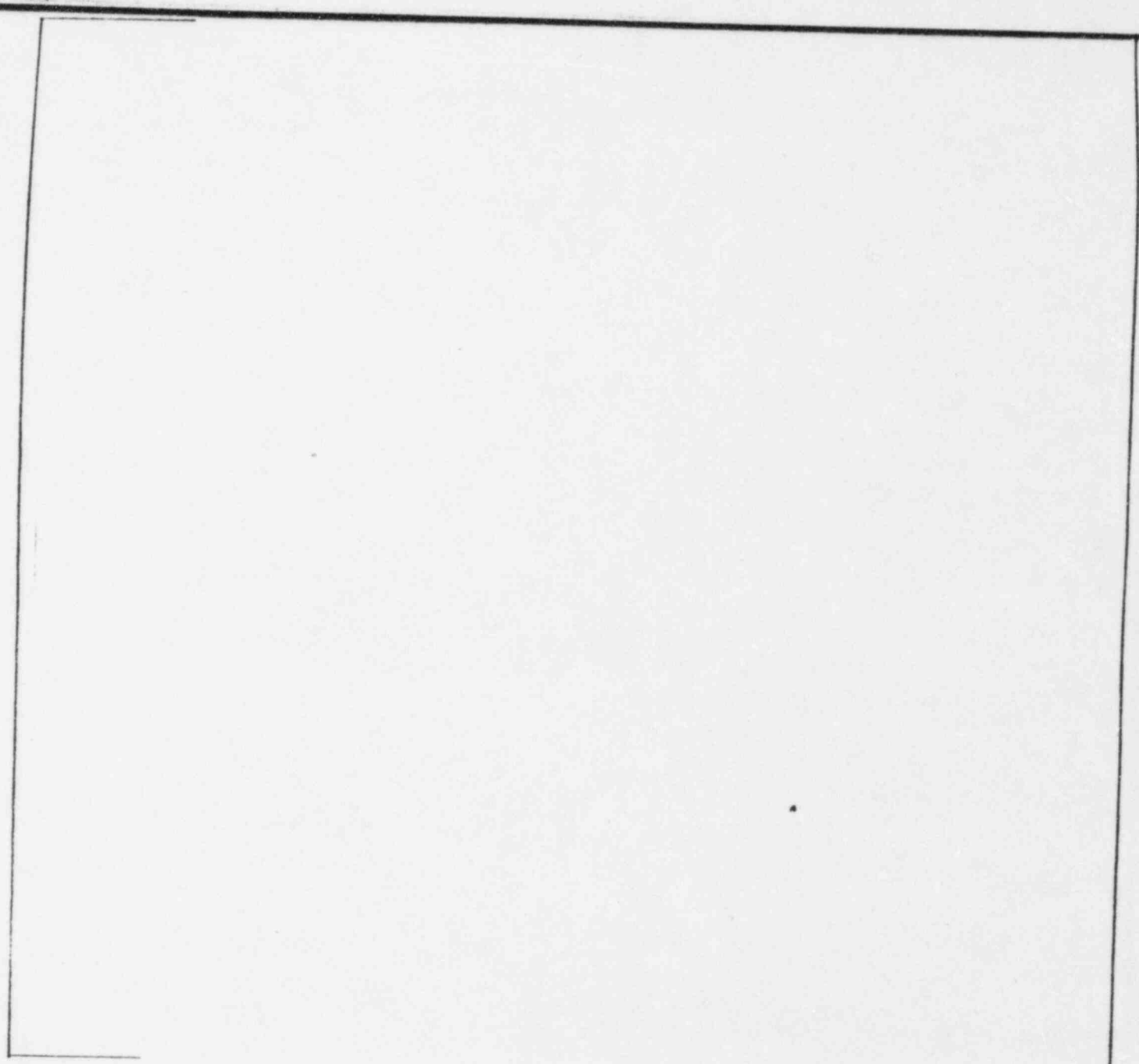

Fig. 5.5 [ ]Model Geometry with[ ]Circumferential Crack -[ ] +a,c,e

Fig. 5-6 [ ]Model Geometry with [ ]Circumferential Crack

+a,c,e
rack

CRACK SURFACE

+a,c,e

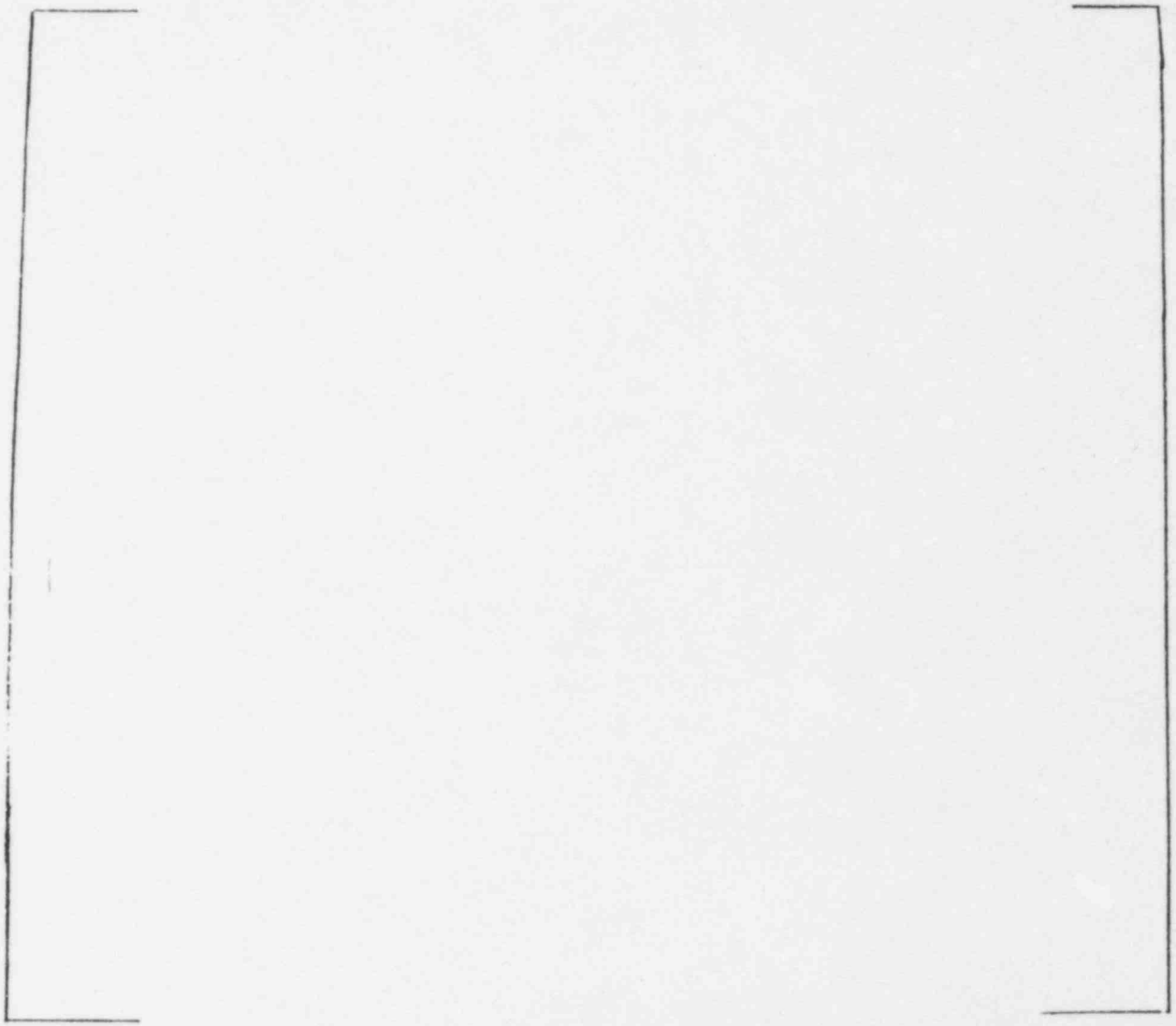

Fig. 5-7 [ ]Model Geometry with [ ]Circumferential Crack -[ ] +a,c,e

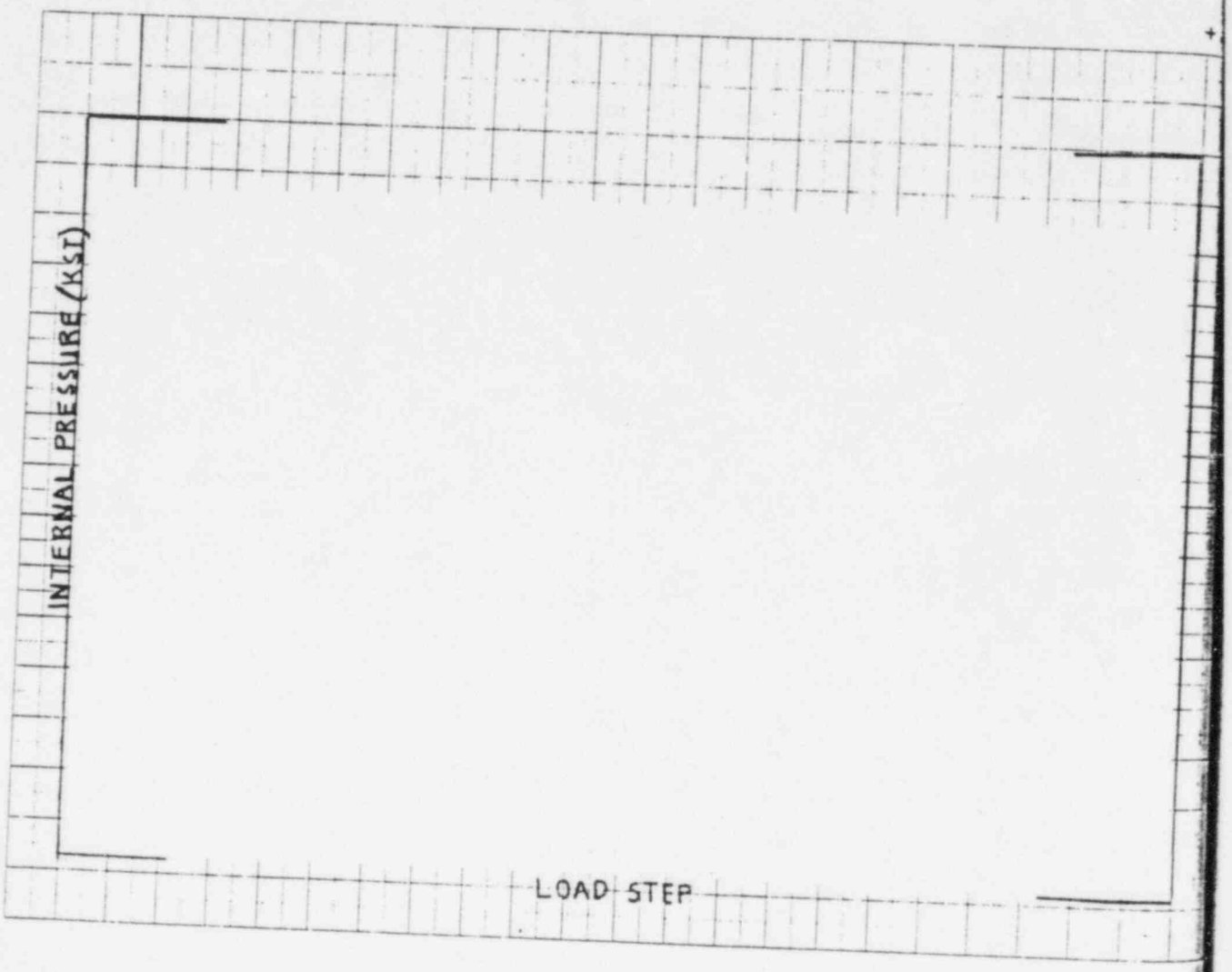

FIGURE 5-8 PRESSURE APPLIED RADIALLY TO INSIDE PIPE WALL

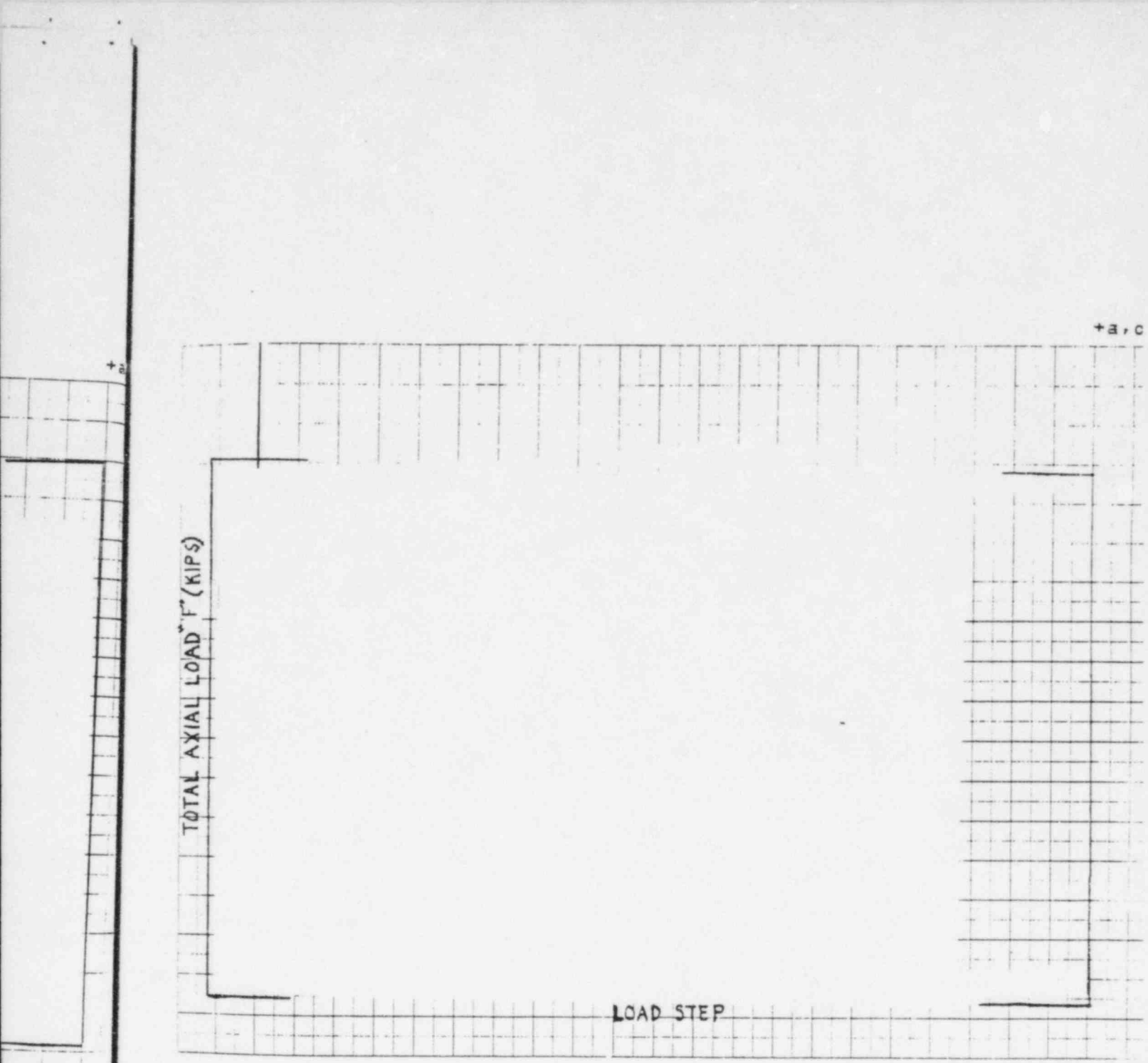

FIGURE 5-9 AXIAL LOAD FROM [ ] LINES +a,c,e

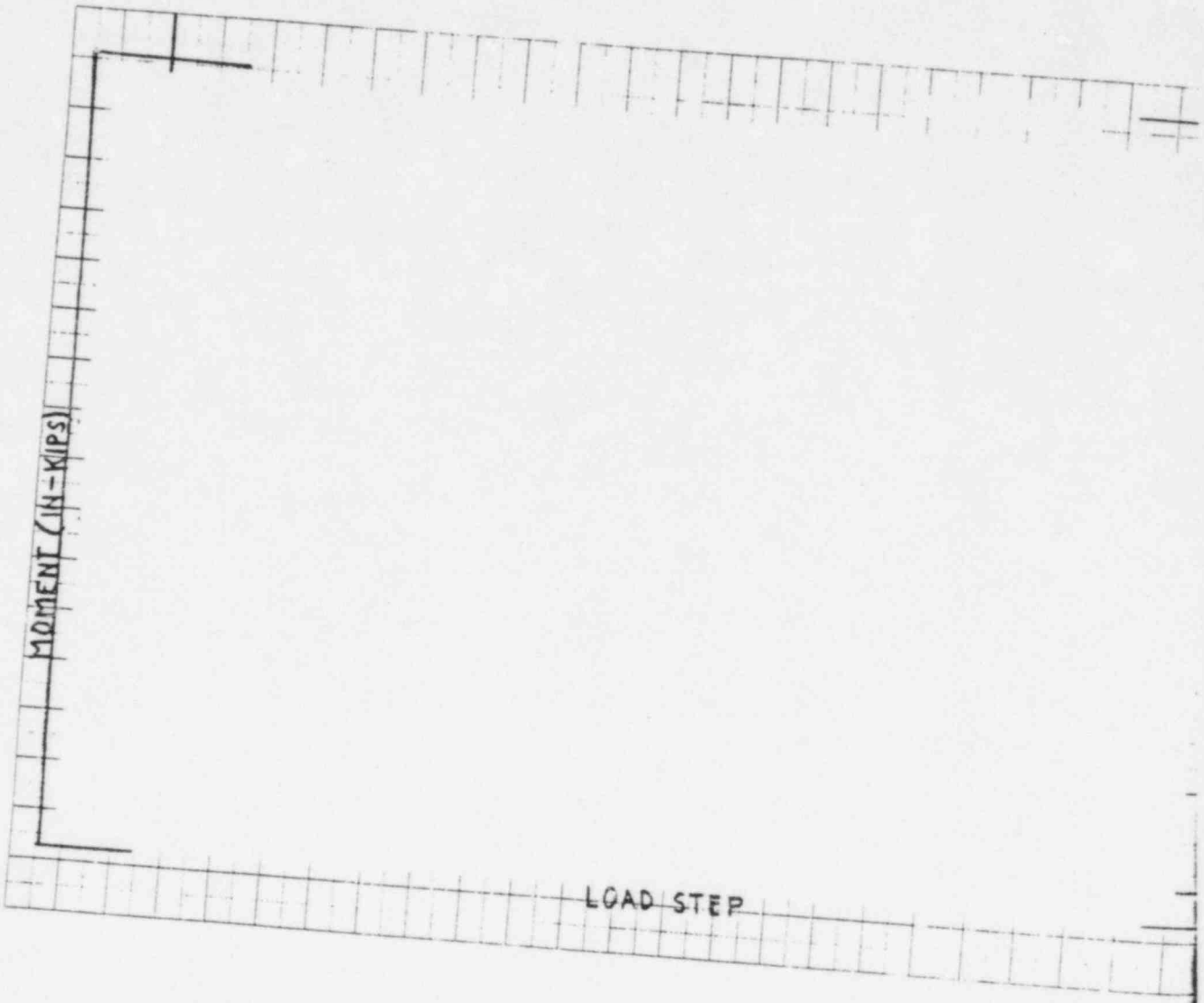

FIGURE 5-10 BENDING MOMENT FROM [ ] +a,c,e

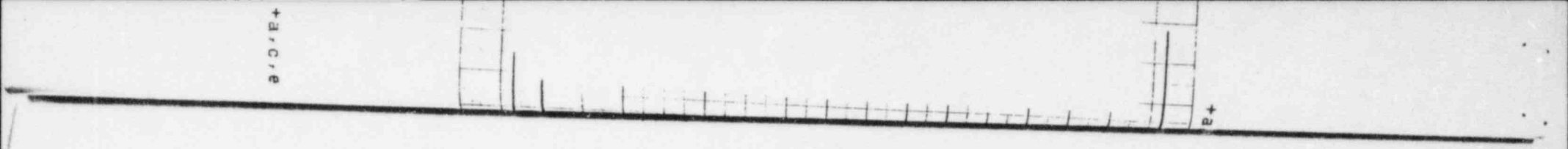

+a,c,e

+a,c,e

+a,c,e

STRESS-KSI

MICRO STRAIN - μ - IN PER INCH

FIGURE 5-11 [ ]STRESS-STRAIN CURVE

+a,c,e

+a,c,e

TGX SURGE LINE-LEAK BEFORE BREAK WITH 7.5 INCH CRACK

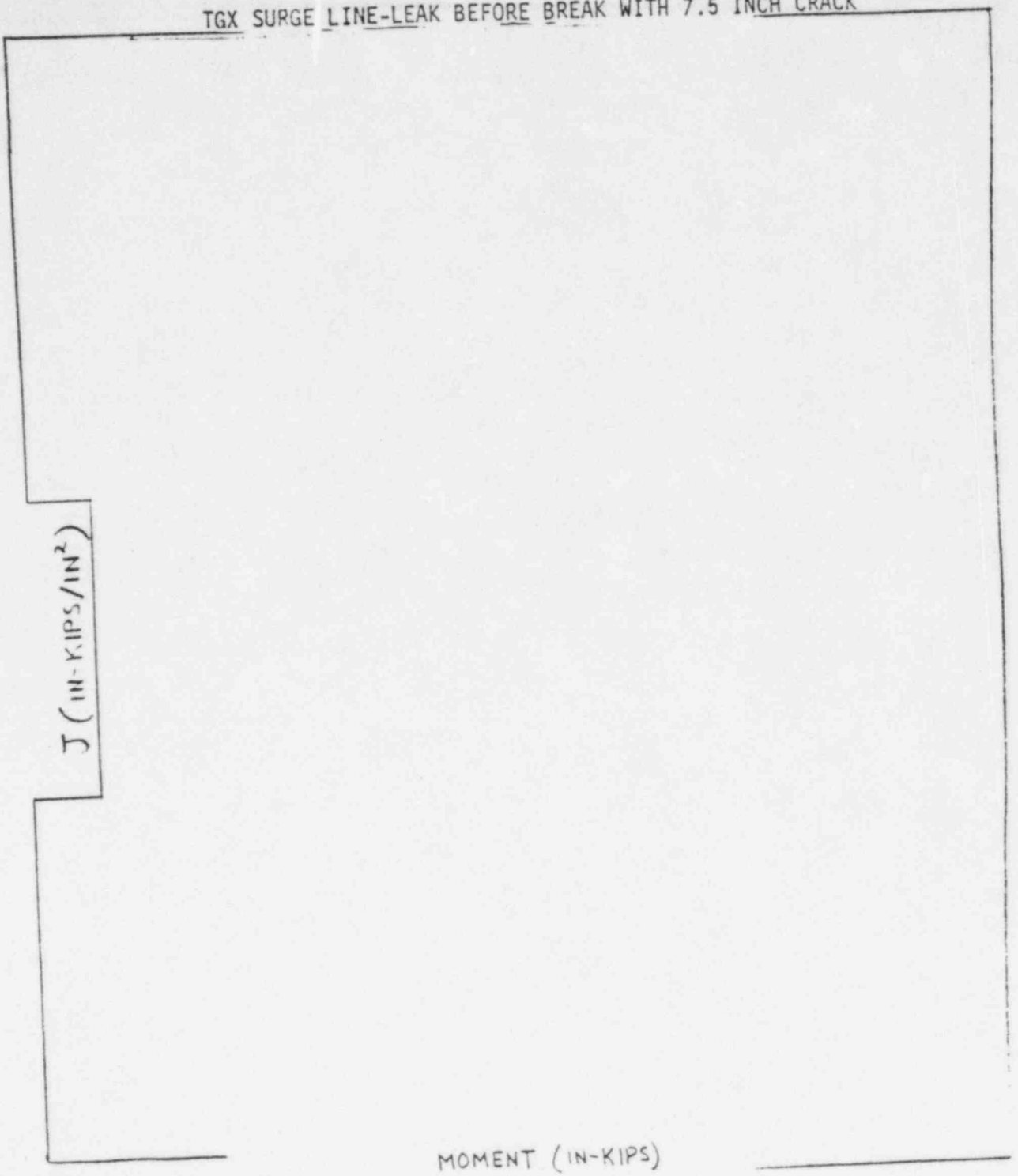

FIGURE 5-12 J-INTEGRAL VERSUS APPLIED MOMENT FOR [ ]

+a,c,e

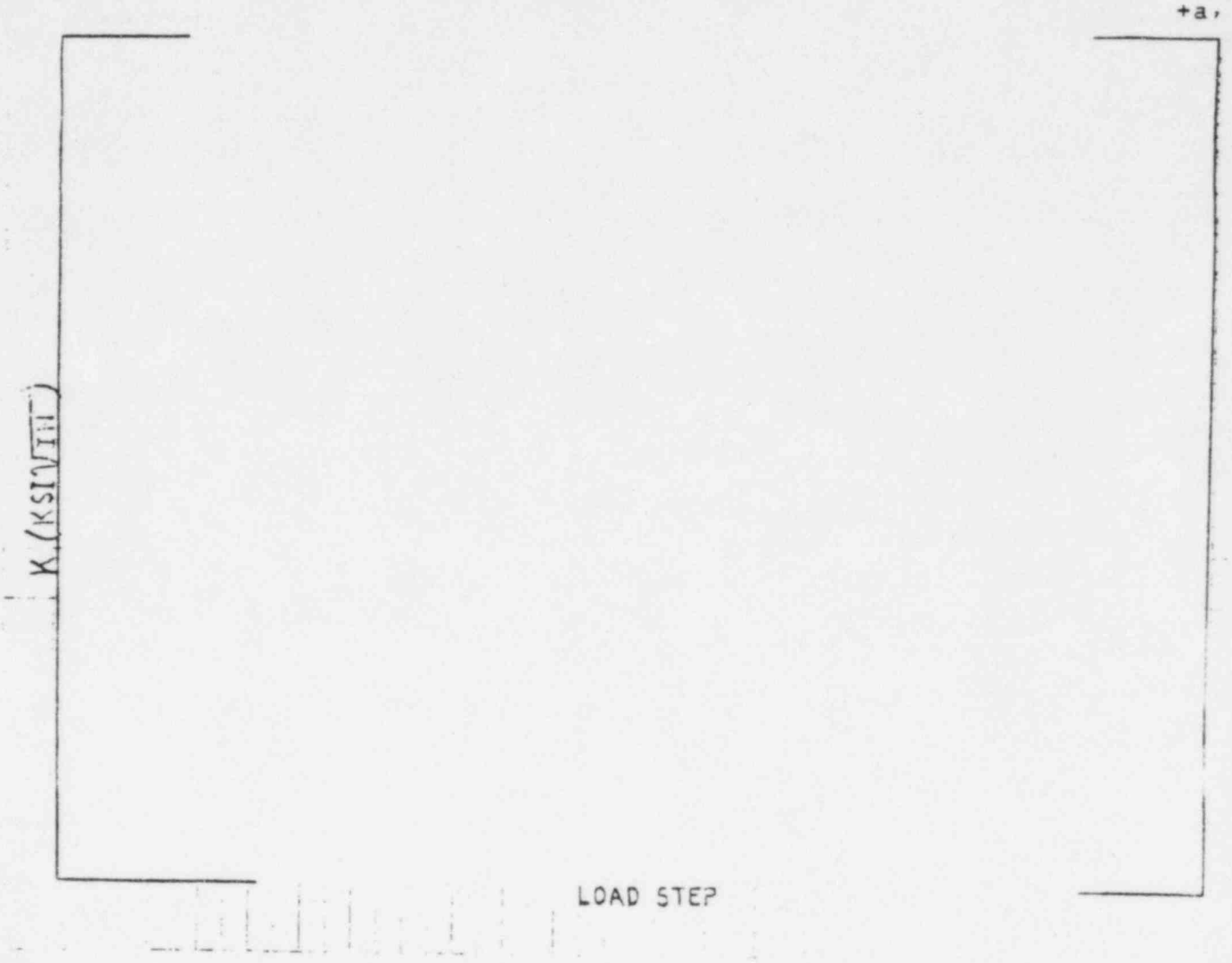

FIGURE 5-13 STRESS INTENSITY FACTORS FROM [ ] COMPARED WITH THE STRESS INTENSITY FACTORS USING LINEAR ELASTIC FRACTURE MECHANICS HAND CALCULATIONS +a,c,e

TABLE 5-1 COMPARISON OF[ ]RESULTS WITH HAND CALCULATIONS +a,c,

6.0 LEAK RATE PREDICTIONS

6.1 INTRODUCTION

Detailed fracture mechanics analysis has shown that through-wall cracks in the surge line would remain stable and not cause a gross failure of this RCS component. If such a through-wall crack did exist, it would be desirable to detect the leak rate such that the plant could be brought to a safe shutdown condition. The purpose of this section is to discuss the method which will be used to predict the flow through such postulated cracks and present the leak rate calculation results for a [ ] through wall circumferential crack. The mechanical stability of the [ ] crack was shown in Section 5.0. +a,c,e +a,c,e

6.2 GENERAL CONSIDERATIONS

The flow of hot pressurized water through an opening to a lower back pressure causes flashing which can result in choking. For long channels where the ratio of the channel length, L, to hydraulic diameter, D_H, (L/D_H) is greater than [ ] both choking and frictional effects must be considered. In this situation the flow can be described as being single phase through the channel until the local pressure equals the saturation pressure of the fluid. At this point, the flow beings to flash and choking occurs. Pressure losses due to momentum changes will dominate for L/D_H<[ ] However, for large L/D_H values, friction pressure drop will become important and must be considered along with the momentum losses due to flashing. +a,c,e +a,c,e

6.3 CALCULATION METHOD

The basic method used in the leak rate calculations is the method developed by [+a,c,e

]

The flow rate through a crack was calculated in the following manner. Figure 6-1 from [ ] was used to estimate the critical pressure, Pc, for the surge line enthalpy condition and an assumed flow. Once Pc was found for a given mass flow, the stagnation presure upstream of the choked plane was found from Figure 6-2 of [ ] For all cases considered, since L/D_H>[ ] Pc/Po = [ ] Therefore, this method will yield the two-phase pressure drop due to momentum effects as illustrated in Figure 6-3. Now using the assumed flow rate G, the frictional pressure drop can be calculated using

+a,c,e

+a,c,e

+a,c,e

[ ] (6-1) +a,c,e

+a,c,e

where the friction factor f is determined using the [ ] for which the crack relative roughness, ε, was obtained from fatigue crack data on stainless steel samples. The relative roughness value used in these calculations was [ ] +a,c,e

The frictional pressure drop using Equation (6-1) is then calculated for the assumed flow and added to the [ ] to obtain the total pressure drop from the primary system to the atmosphere. That is +a,c,e

+a,c,e

Surge Line Pressure - 14.7 = ΔP_T = [ ] (6-2)

for a given assumed flow G. If the right-hand-side of Equation (6-2) does not agree with the pressure difference between the surge line and atmosphere, then the procedure is repeated until Equation (6-2) is satisfied to within an acceptable tolerance and this then results in the flow value through the crack. This calculational procedure has been recommended by [ ] calculation. The +a,c,e

leak rates obtained by this method have been compared in [ ] with experimental results. The comparison indicated that the method predicts leak rate with acceptable accuracy [ ] +a,c,e

6.4 CRACK OPENING AREAS

Figure 6-4 plots the shape of one quarter of the opened crack at the inside and outside radii of the pipe, at [ ] when the pressure and axial loadings reach their [ ]. Figure 6-5 is a similar plot for [ ] when a moment of [ ] Table 6-1 presents the coordinates and displacements [ ] used to generate the two Figures. The area under each curve is found by numerical integration. Multiplying each of the four areas by 4 gives the total areas of the cracks at the inside and outside radii of the pipe, for the two loading conditions. Two leak rates will be calculated using the areas. These are: +a,c,e +a,c,e +a,c,e +a,c,e +a,c,e

(a) the leak rate for the loading condition where there is [ ] (Load A) +a,c,e

(b) the leak rate for the loading condition where there is [ ] +a,c,e

For load step 3, the crack areas are as follows:

+a,c,e

Inside Area, A_{3i} [ ]
Outside Area, A_{3o}

To calculate the areas for Load A, above, the areas A_{3i} and A_{3o} for step 3 must be reduced so as to exclude the [ ] [ ] Areas A_{3i} and A_{3o} are therefore reduced by a factor of [ ] to obtain the leak areas A'_{3i} and A'_{3o} for Load A. +a,c,e +a,c,e +a,c,e +a,c,e

+a,c,e

A'_{3i} = [ ] (A_{3i}) [ ]

A'_{3o} = [ ] (A_{3o}) [ ]

[+a,c,e

]

Flow rates are calculated by the [+a,c,e
[ ] for Load A and Load B. Flow areas are determined by averaging the crack areas on the inside and outside radii of the pipe. The average area for Load Case A is [ ] $in.^2$. The average +a,c,e
area for Load Case B is [ ] $in.^2$. +a,c,e

6.5 LEAK RATE RESULTS

Using the [ ] method gives a [ ] lb/sec leak rate for Load Case A +a,c,e
[ ] For Load Case B, the method gives [ ] +a,c,e
]

Case B is considered more realistic since it [+a,c,e
] This calculated leak rate is significantly higher than the leak detection criterion of 1 gpm (Regulatory Guide 1.45).

6.6 REFERENCES

+a,c,e

6-1 [

6-2

6-3

]

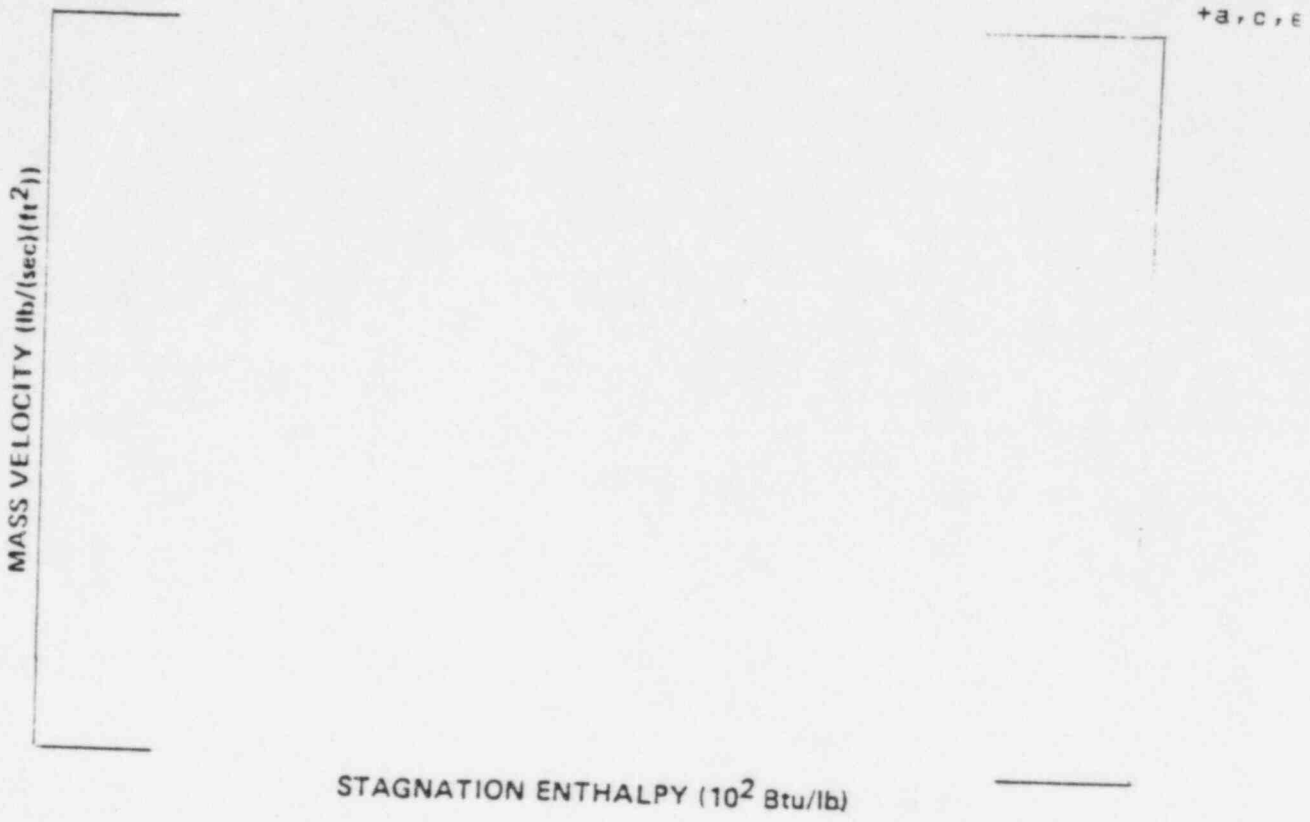

Figure 6-1 Analytical Predictions of Critical Flow Rates of Steam-Water Mixtures

+a,c

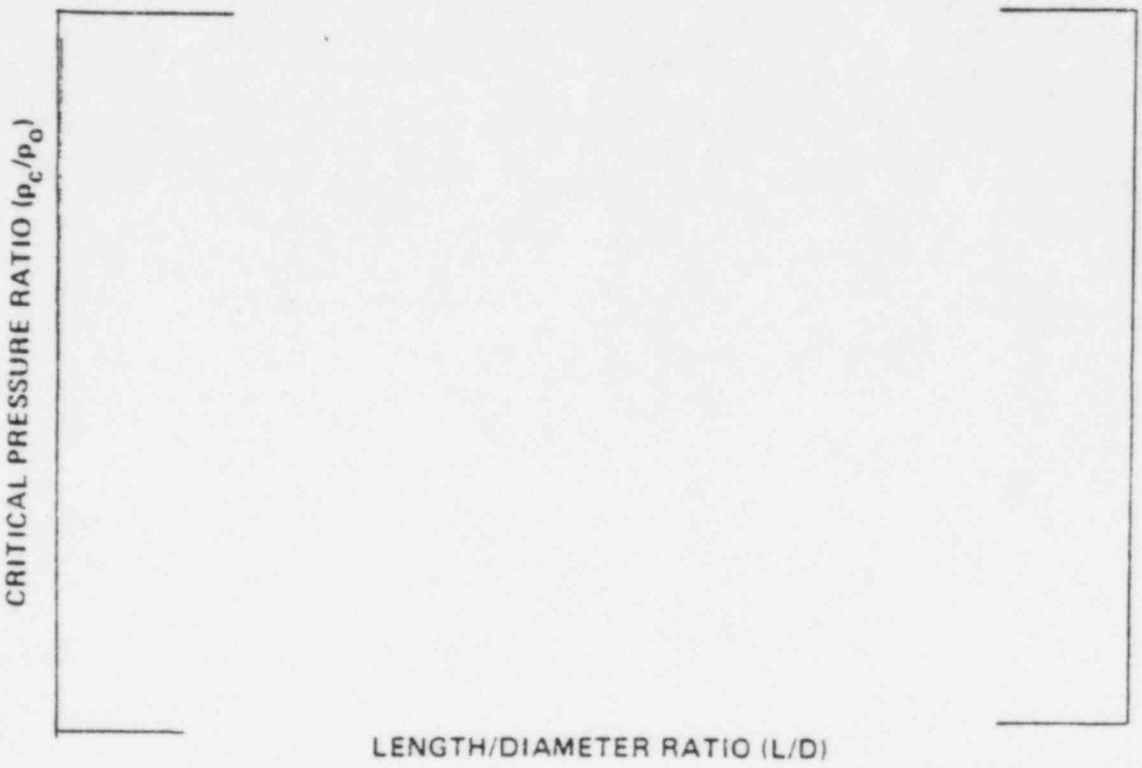

Figure 6-2 Critical or Choked Pressure Ratio as a Function of L/D

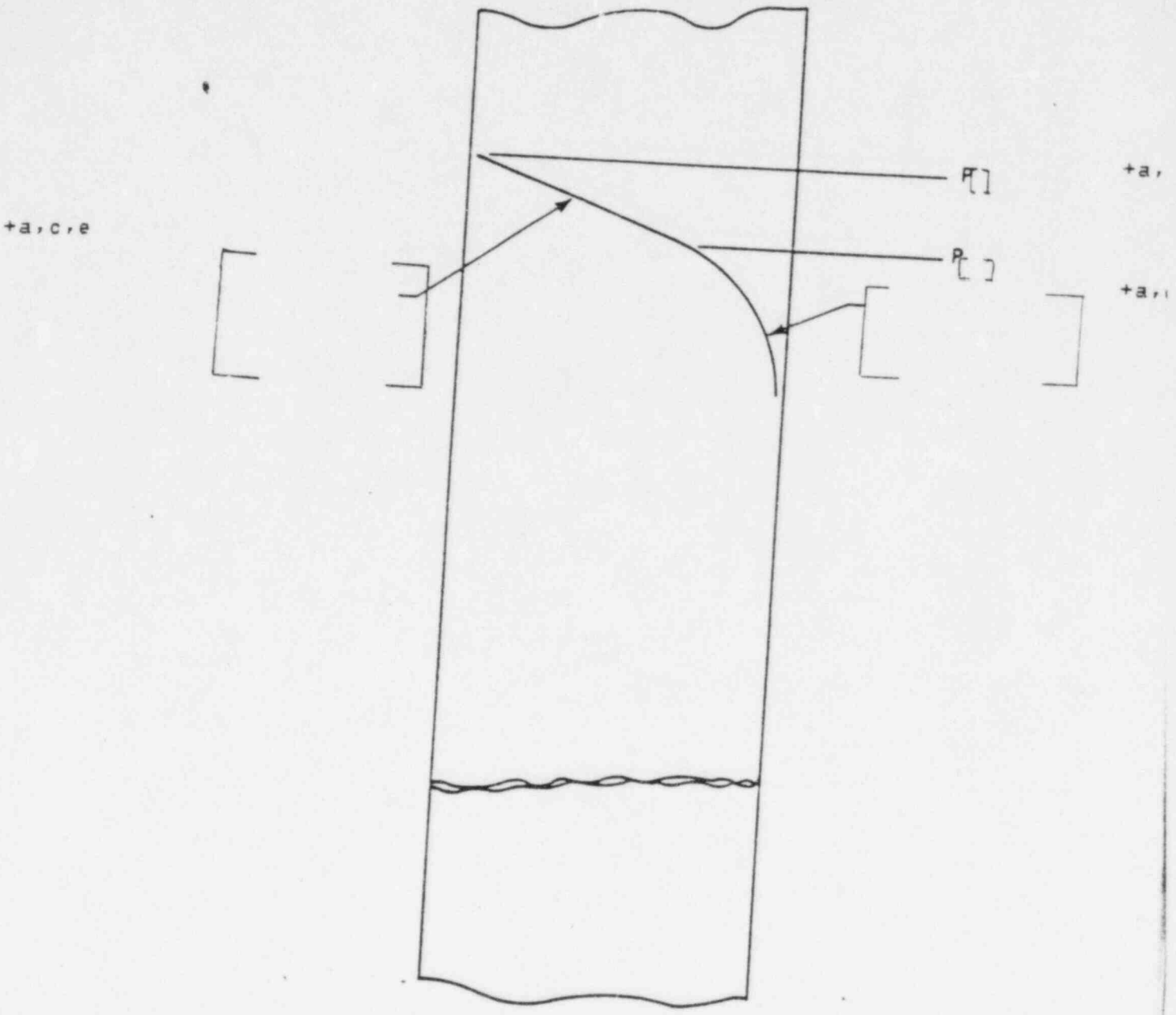

Figure 6-3 Idealized Pressure Drop Profile Through a Postulated Crack

+a,c,

c,e

c,e

X-DISPLACEMENT (INCHES)

ARC LENGTH (INCHES)

Figure 6-4 One Quarter of the Crack Opening at[ ] Pressure +a,c,e
plus Axial Load

+a,c,e

X-DISPLACEMENT (INCHES)

ARC LENGTH (INCHES)

Figure 6-5 One Quarter of the Crack Opening at [ ] combined with [ ]

+a,c,e

+a,c,e

TABLE 6-1

CRACK [ ] DISPLACEMENTS +a,c,e

[+a,c,e]

7.0 THERMAL TRANSIENT STRESS ANALYSIS

The thermal transient stress analysis was performed to obtain the through wall stress profiles for use in the fatigue crack growth analysis of Section 8.0. The through wall stress distribution for each transient was calculated for i) the time corresponding to the maximum inside surface stress and, ii) the time corresponding to the minimum inside surface stress. These two stress profiles are called the maximum and minimum through wall stress distribution, respectively for convenience. The constant stresses due to [+a,c,e] loadings were superimposed on the through wall cyclical stresses to obtain the total maximum and minimum stress profile for each transient. The through wall stress distribution was initially calculated by conservative simplified methods for all transients. Based on these results, the [+a,c,e] stress analysis was performed for a few severe transients to reduce the conservatism of simplified methods.

7.1 CRITICAL LOCATION FOR FATIGUE CRACK GROWTH ANALYSIS

The surge line stress report[3-1], design thermal transients (Section 7.2), 1-D analysis data on surge line thermal transient stresses (based on ASME Section III NB3600 rules) and the geometry were reviewed to select the worst location for the fatigue crack growth analysis. The [+a,c,e] was determined to be the most critical location for the fatigue crack growth evaluation. This location is selected as the worst location)same as determined in Table 3-1) based on the following considerations:

i) [+a,c,e
ii)
iii)
iv)]

7.2 DESIGN TRANSIENTS

The transient conditions selected for this evaluation are based on conservative estimates of the magnitude and the frequency of the temperature fluctuations resulting from various operating conditions in the plant. These are representative of the conditions which are considered to occur during plant operation. The fatigue evaluation based on these transients provide confidence that the component is appropriate for its application over the design life of the plant. A total of [ ] envelope thermal transients was +a,c,e developed for the surge line by considering all the normal operating and upset transients in accordance with design specifications[7-1] and the applicable system standard design criteria documents[7-2, 7-3]. Some of the data of the applicable criteria documents was refined to more closely represent the transients and to reduce the conservatism in fluid temperature fluctuations and the rate of change of fluid temperature. The thermal transients considered for the fatigue crack growth evaluation are listed in Table 7-1.

7.3 SIMPLIFIED STRESS ANALYSIS

The simplified analysis method was used to develop conservative maximum and minimum linear through wall stress distributions due to thermal transients. In this method, a 1-D computer program was used to perform the thermal analysis to determine the through wall temperature gradients as a function of time. The inside surface stress was calculated by the following equation which is similar to the transient portion of ASME Section III NB3600, Eq. 11:

[+a,c,e]

[+a,c,e]

[

] The maximum and minimum +a,c,e
inside surface stresses were searched from the S_i values calculated for each time step of the transient solution.

The outside surface stresses corresponding to maximum and minimum inside stresses were calculated by the following equations:

[+a,c,e]

where,

[+a,c,e]

The following material properties were used for the pipe [ ] and nozzle [ ] safe end in the above stress calculations. +a,c,e +a,c,e

[ ] +a,c,e

The maximum and minimum linear through wall stress distribution for each thermal transient was obtained by [ ] The simplified analysis discussed in this section was performed for all minor thermal transients of Table 7-1 [ ] +a,c,e +a,c,e

] The simplified method provides more conservative crack growth.

7.4 [ ] STRESS ANALYSIS +a,c,e

As mentioned earlier, [ ] is the worst location for fatigue crack growth analysis. A schematic of the surge line and nozzle geometry at this location[7-4, 7-5] is illustrated in Figure 7.2. The computer model developed for this location is shown in Figure 7-2. The model was developed for [ ]. It included [+a,c,e

]

[ ]

+a

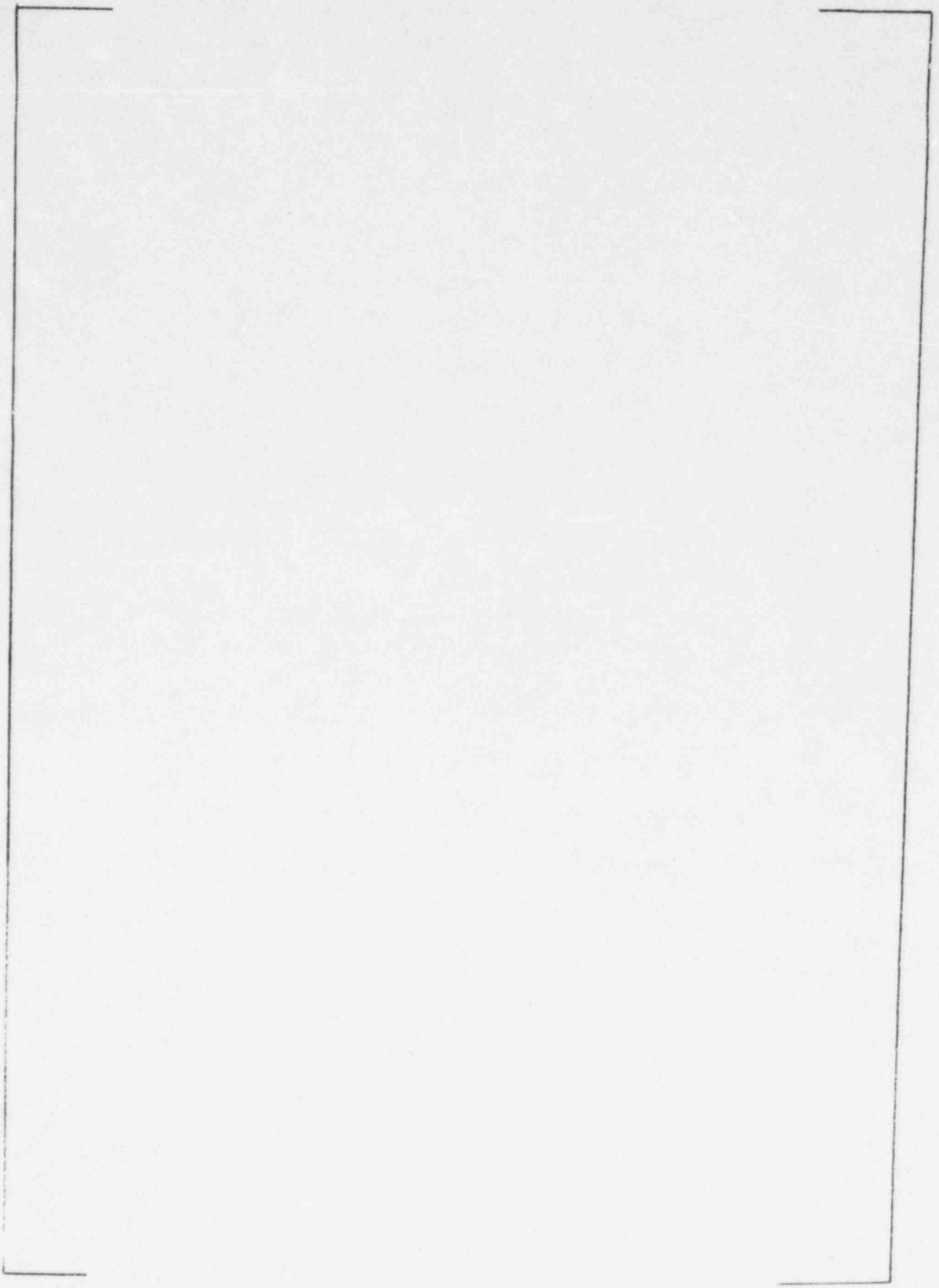

+a,c,e

7.5 OBE LOADS

In addition to thermal transients, cyclical stresses due to OBE event were also used for the fatigue crack growth evaluation. The maximum and minimum inside and outside OBE stresses were calculated from the OBE

loading case computer run of the stress report[3-1]. A total of 20 OBE events (with 20 cycles per each event) are considered for fatigue crack growth in accordance with[7-1]. The OBE stresses are as follows:

	Inside Surface Stress (ksi)	Outside Surface Stress (ksi)	
Maximum	[	]	+a,c,e
Minimum			

7.6 TOTAL STRESS FOR FATIGUE CRACK GROWTH

The total through wall stress at a section was obtained by superimposing the pressure load stresses and the stresses due to [+a,c,e

] Thus, the total stress for fatigue crack growth at any point is given by the following equation:

$$\text{Total for Fatigue Crack Growth} = \left[\right] \quad (7.7)$$ +a,c,e

The average pipe wall temperature during the steady state and random fluctuation transients is smaller than the normal operating temperature of [ ] The average pipe wall temperature for these transients was assumed to be that given by the following relation, +a,c,e

$$T_{avg} = [\quad] \quad (7.8)$$ +a,c,e

Thermal expansion moments for these transients were reduced for the average wall temperature calculated by Eq. 7.8 and the lower coefficient

of thermal expansion value for the pipe material in accordance with the ASME Code[7-8]. The revised moments were calculated by the following equation.

$$M_n = [\quad] \qquad (7.9) \qquad +a,c,e$$

where,

+a,c,e

[

]

for calculating the total stresses, are summarized in Table 7-4.

7.7 REFERENCES

7-1 [ ]

7-2 [ ]

7-3 [ ]

7-4 Westinghouse TGX Surge Line Fabrication Drawings:

[ ]

7-5 [ ]

[ ]

7-6 [ ]

7-7 [ ]

7-8 ASME Section III, Division 1-Appendices, 1983 Edition, July 1, 1983.

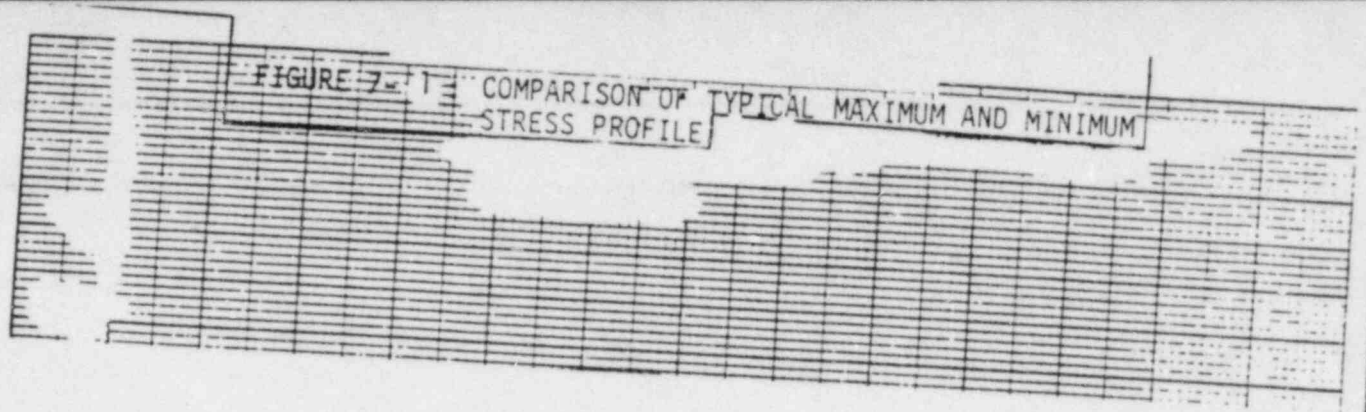

FIGURE 7-1 COMPARISON OF TYPICAL MAXIMUM AND MINIMUM STRESS PROFILE

+a,c,e

SCHEMATIC OF [ ]

FIGURE 7-2

TEMPERATURE LOADING AND FILM COEFFICIENTS
WERE APPLIED TO INNER SURFACE [

]

+a,c,e

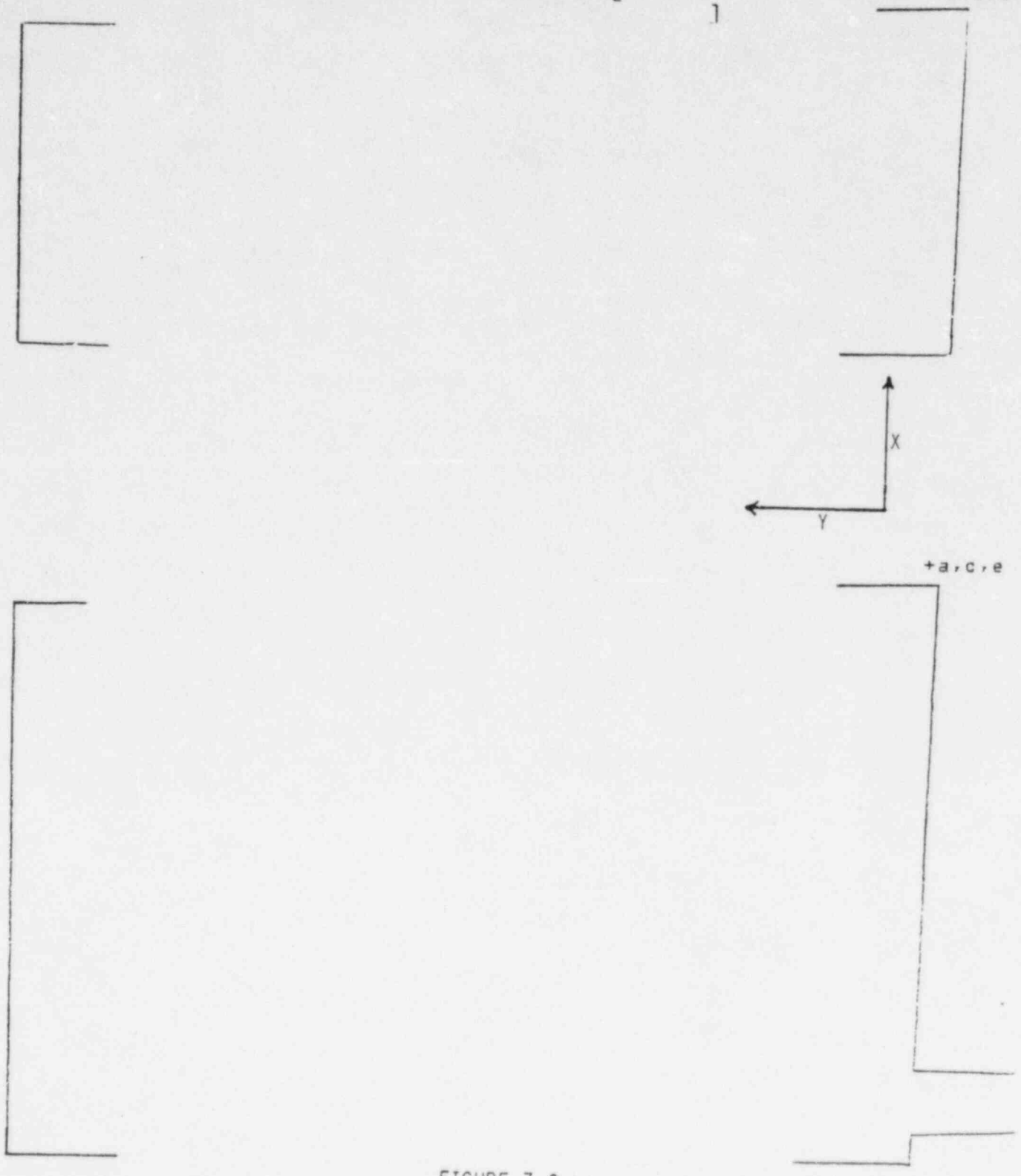

FIGURE 7-3

[ ] MODEL [

]

+a

FIGURE 7-4 = MAXIMUM AND MINIMUM STRESS PROFILE[

+a,c

FIGURE 7- 5 : MAXIMUM AND MINIMUM STRESS [+a,c,e

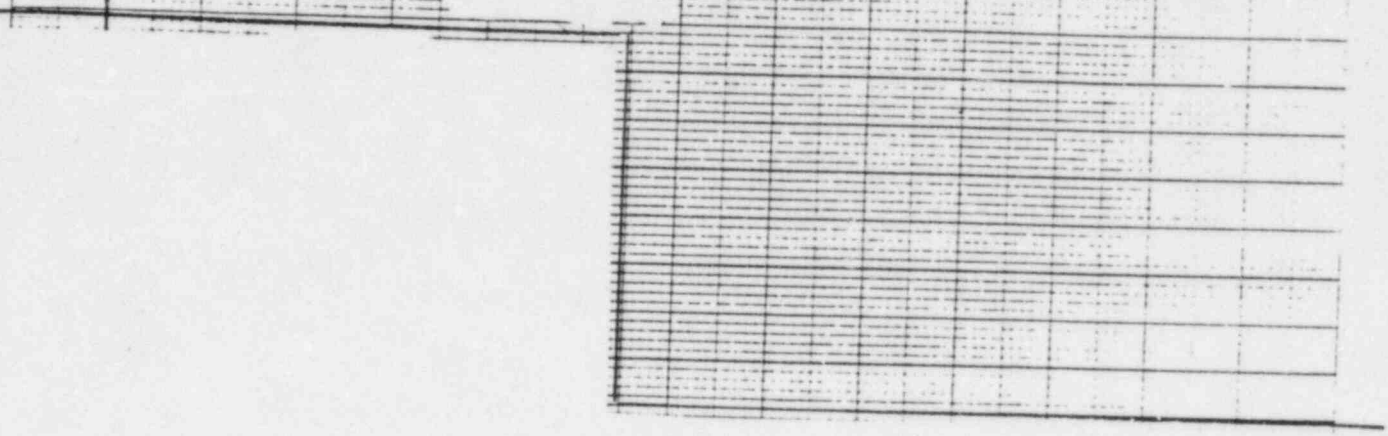

]

+a

FIGURE 7-6 : MAXIMUM AND MINIMUM STRESS PROFILE [+a,c,

]

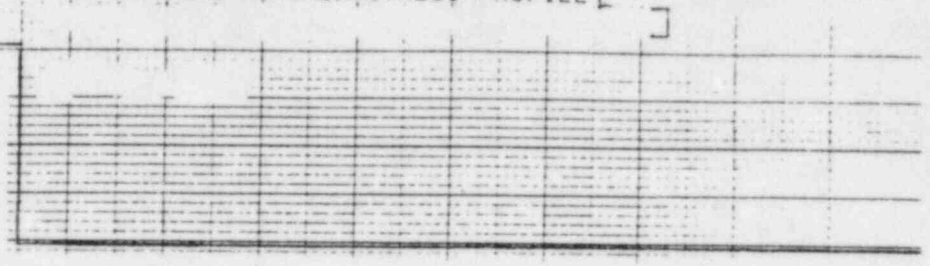

FIGURE 7-7 : MAXIMUM AND MINIMUM STRESS PROFILE [

]

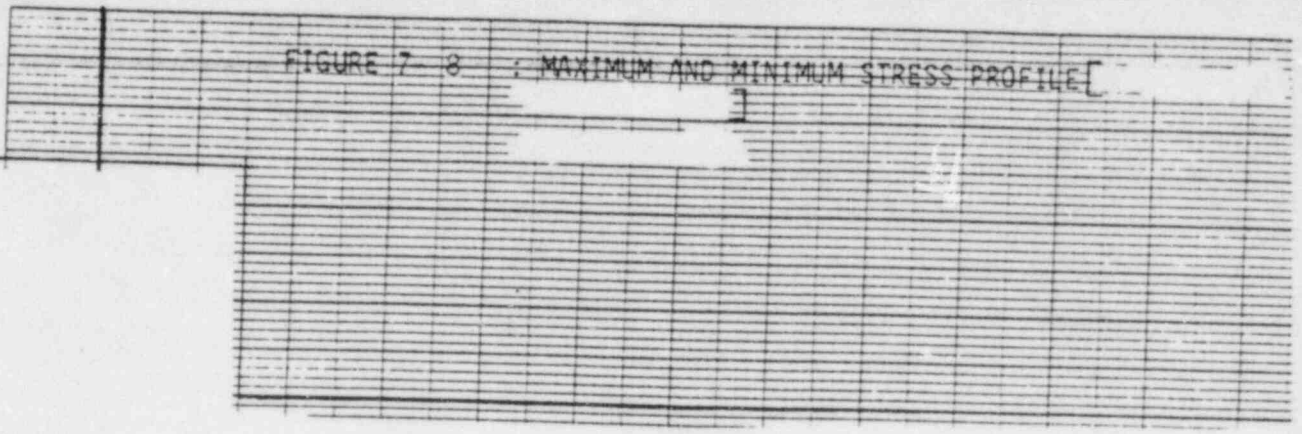

FIGURE 7-8 : MAXIMUM AND MINIMUM STRESS PROFILE[ ]

FIGURE 7-9 : MAXIMUM AND MINIMUM STRESS PROFILE[

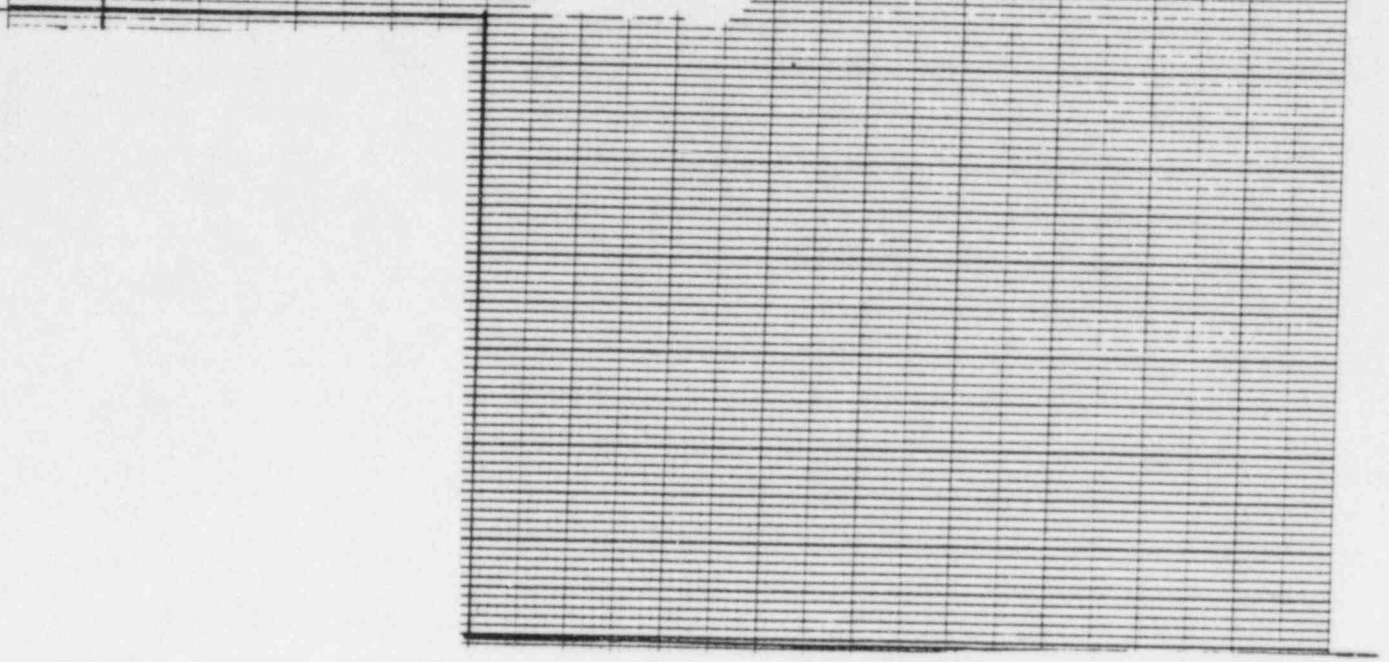

]

FIGURE 7-10 : MAXIMUM AND MINIMUM STRESS PROFILE

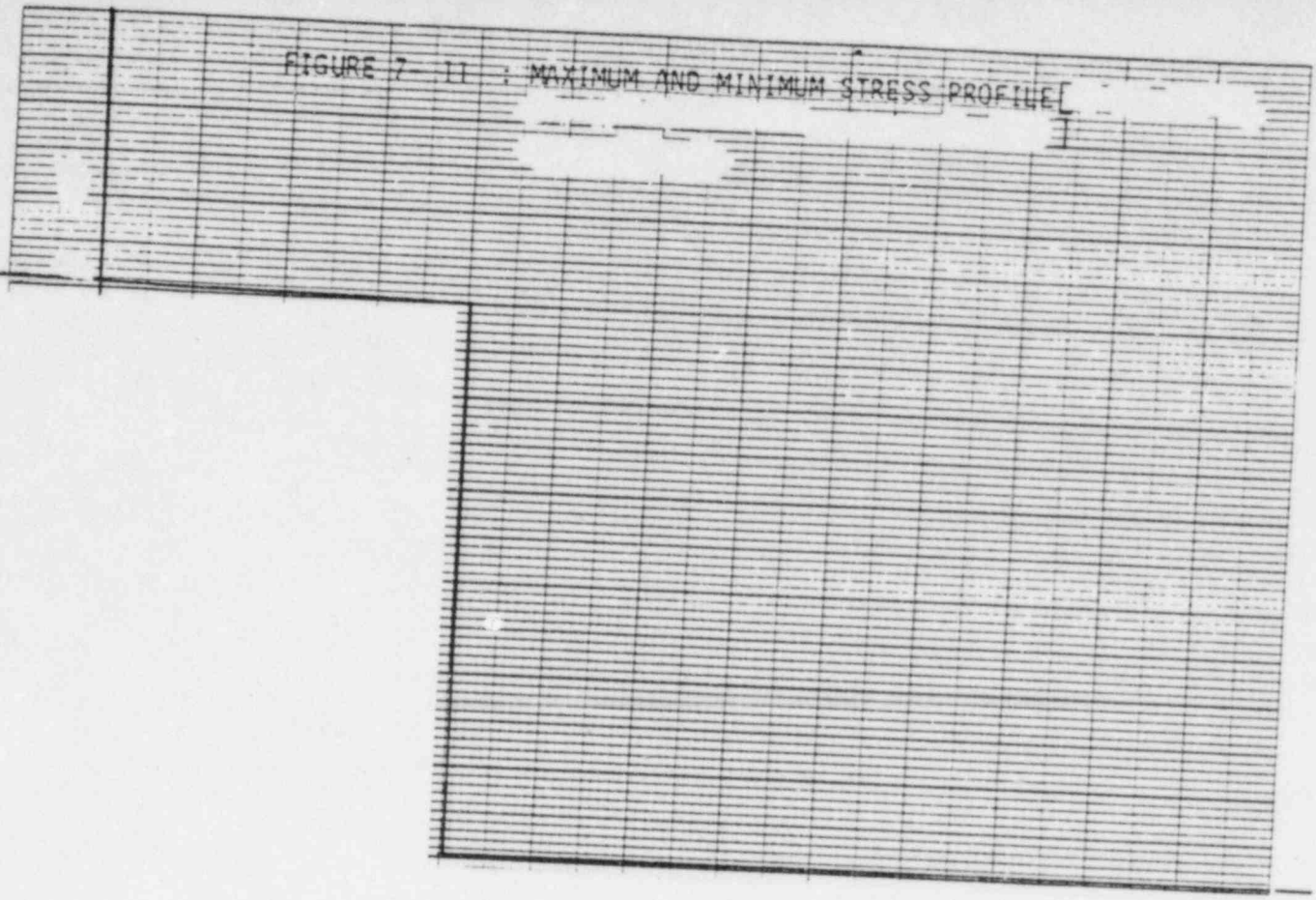

FIGURE 7- 11 : MAXIMUM AND MINIMUM STRESS PROFILE

FIGURE 7-12 MAXIMUM AND MINIMUM STRESS PROFILE[

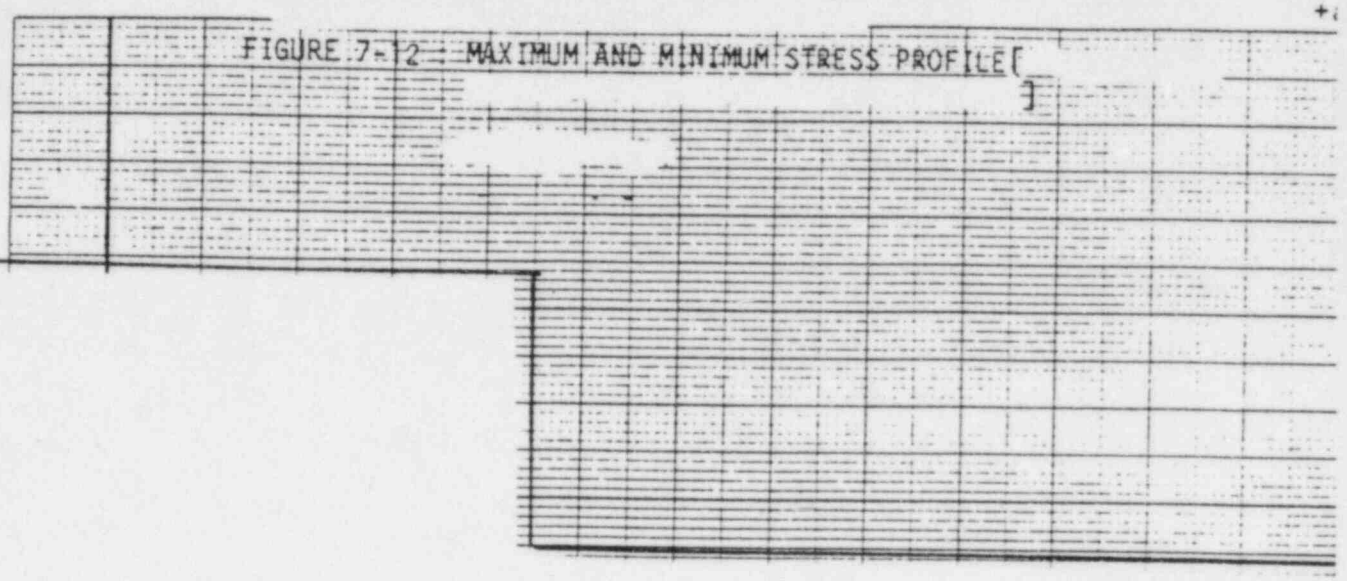

]

+a

FIGURE 7-13: MAXIMUM AND MINIMUM STRESS PROFILE

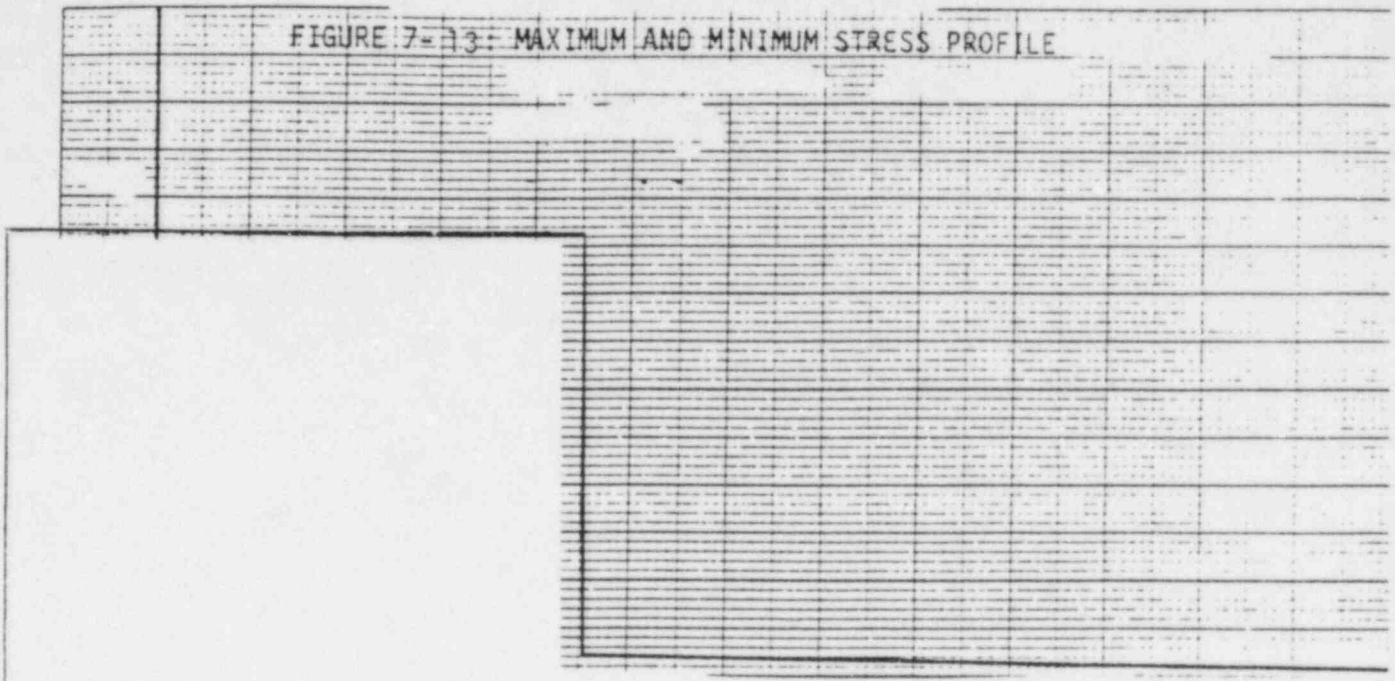

a,c,

TABLE 7-1

THERMAL TRANSIENTS CONSIDERED FOR FATIGUE CRACK GROWTH EVALUATION

Trans. No.	Description	No. of Occurrences	Trans. No.	Description	No. of Occurrenc
					+a,

TABLE 7-2

THERMAL TRANSIENT STRESSES BY SIMPLIFIED ANALYSIS

Transient No.	Description	Number of Occurrences	Max Peak Stress (S_p) Time (sec)	Max Peak Stress (S_p) Inside Max S_p (ksi)	Max Peak Stress (S_p) Corresponding Outside S_p (ksi)	Min Peak Stress (S_p) Time (sec)	Min Peak Stress (S_p) Inside Min S_p (ksi)	Min Peak Stress (S_p) Corresponding Outside Min S_p (ksi)
								+a,c,e

+Tension
-Compression

TABLE 7-3

MATERIAL PROPERTIES

Material Number	Description	Coefficients	EA	Properties* ALPX**	KXX	CP	DENS	XNU

+a,c,e

TABLE 7-4

[ ]STRESSES FOR +a,c,e

FATIGUE CRACK GROWTH

Transient No.	Loading	Axial Force Fl (k)	Bending Moment BM (ft-k)	Stress (ksi) Inside	Stress (ksi) Outside
[					] +a,c,e

8.0 FATIGUE CRACK GROWTH ANALYSIS

The fatigue crack growth analysis was performed to determine the effect of the design thermal transients in Table 7-1 along with the OBE Load transient. The analysis was performed for two cross sections of the model [+a,c,e] A range of crack depths were postulated [ ] and each postulated crack was subjected to the transients in Table 7-1 as well as the OBE Load transient.

8.1 ANALYSIS PROCEDURE

The fatigue crack growth analyses presented herein were conducted in the same manner as suggested by Section XI, Appendix A of the ASME Boiler and Pressure Vessel Code. The analysis procedure involves assuming an initial flaw exists at some point and predicting the growth of that flaw due to an imposed series of stress transients. The growth of a crack per loading cycle is dependent on the range of applied stress intensity factor ΔK_I, by the following relation:

$$\frac{da}{dN} = C_o \Delta_I^{\,n} \qquad (8\text{-}1)$$

where "Co" and the exponent "n" are material properties, and ΔK_I is defined later, in Equation (8-3). For inert environments these material properties are constants, but for some water environments they are dependent on the level of mean stress present during the cycle. This can be accounted for by adjusting the value of "Co" and "n" by a function of the ratio of minimum to maximum stress for any given transient, as will be discussed later. Fatigue crack growth properties of stainless steel in a pressurized water environment have been used in the analysis.

The input required for a fatigue crack growth analysis is basically the information necessary to calculate the parameter ΔK_I, which depends on crack and structure geometry and the range of applied stresses in the area where the crack exists. Once ΔK_I is calculated, the growth due to that

particular cycle can be calculated by Equation (8-1). This increment of growth is then added to the original crack size, the ΔK_I adjusted, and the analysis proceeds to the next transient. The procedure is continued in this manner until all the transients have been analyzed.

The crack tip stress intensity factors (K_I) to be used in the crack growth analysis were calculated using an expression which applies for a semi-elliptic surface flaw in a cylindrical geometry [8-1.]

The stress intensity factor expression was taken from Reference 8-1 and was calculated using the actual stress profiles [+a,c,e] The maximum and minimum stress profiles corresponding to each transient were input, and each profile was fit by a third order polynomial:

$$\sigma(x) = A_0 + A_1 \frac{x}{t} + A_2 \left(\frac{x}{t}\right)^2 + A_3 \left(\frac{x}{t}\right)^3 \qquad (8\text{-}2)$$

The stress intensity factor $K_I(\phi)$ was calculated at the deepest point of the crack using the following expression:

+a,c,e

(8-3)

Calculation of the fatigue crack growth for each cycle was then carried out using the reference fatigue crack growth rate law determined from consideration of the available data for stainless steel in a pressurized water environment. This law allows for the effect of mean stress or R ratio ($K_{I\ min}/K_{I\ max}$) on the growth rates.

The reference crack growth law for stainless steel in a pressurized water environment was taken from a collection of data [8-2] since no code curve is available, and it is defined by the following equation:

$$\frac{da}{dN} = (0.0054 \times 10^{-3})\ (K_{eff})^{4.48} \qquad (8\text{-}4)$$

where $K_{eff} = (K_{Imax})\ (1-R)^{1/2}$

$$R = \frac{K_{I\ min}}{K_{I\ max}}$$

$\frac{da}{dN}$ = crack growth rate in micro-inches/cycle

8.2 RESULTS

Fatigue crack growth analyses were carried out for two cross sections of the model, [ ] +a,c,e
Analyses were completed [ ] for a range of postulated flaw sizes +a,c,e
oriented circumferentially, and the results are presented in Tables 8-1 and 8-2. The postulated flaws are assumed to be six times as long as they are deep. Even for the largest postulated flaw of [+a,c,
] the results show that flaw growth through the wall will not occur during the 40 year design life of the plant. For smaller flaws, the flaw growth is significantly lower. For example, a postulated [ ] inch deep flaw +a,c,
will grow to less than 1/2 the wall thickness. These results also confirm operating plant experience. There have been no leaks observed in Westinghouse PWR surge lines in over 400 reactor years of operation.

8.3 REFERENCES

8-1 McGowan, J. J. and Raymund, M., "Stress Intensity Factor Solutions for Internal Longitudinal Semi-Elliptical Surface Flaws in a Cylinder Under Arbitrary Loadings," Fracture Mechanics ASTM STP 677, 1979, pp. 365-380.

8-2 Bamford, W. H., "Fatigue Crack Growth of Stainless Steel Reactor Coolant Piping in a Pressurized Water Reactor Environment," ASME Trans. Journal of Pressure Vessel Technology, February 1979.

TABLE 8-1

FATIGUE CRACK GROWTH RESULTS [+a,c,e

]

INITIAL CRACK LENGTH (IN.)	CRACK LENGTH AFTER YEAR			
	10	20	30	40
[+a,c,e				]

TABLE 8-2

FATIGUE CRACK GROWTH RESULTS [ ] +a,c,e

INITIAL CRACK LENGTH (IN.)	CRACK LENGTH AFTER YEAR				
	10	20	30	40	+a,c,e
[					]

9.0 CONCLUSIONS

A mechanistic fracture evaluation of the South Texas Project pressurizer surge line was performed. The worst location in the pressurizer surge line was identified [+a,c,
] The critical crack length at this location was calculated as [+a,c,
] analysis was performed using a through-wall flaw [+a,c,
] The applied J integral [ ] was calculated +a,c,
corresponding to the maximum applied load including the Safe Shutdown Earthquake load. The applied J integral was shown to be less than $J_{initiation}$ [ ] for the material. These results +a,c,
demonstrate that a [ ] in. crack will remain stable when subjected to +a,c,
maximum loading conditions considering both global and local failure mechanism.

The leakage through a crack [ ] inches long [ ] was calculated as [ ] +a,c,
gpm under the normal operating loads. The South Texas Plant has an RCS pressure boundary leak detection system which is consistent with the requirements of Regulatory Guide 1.45 and can detect leakage of 1 gpm in one hour. Thus, there is a factor of at least [ ] between the calculated leak +a,c,
rate and the South Texas plant leak detection systems capability.

Fatigue crack growth was determined for postulated inside surface flaws using plant design transients. Crack growth results indicated that even a postulated surface flaw which is [ ] of the wall thickness in depth will not +a,c
penetrate the wall over the plant life. Thus, there is no known mechanism which could cause a through-wall crack of the type assumed in the stability calculations.

The incidence of stress corrosion cracking is eliminated by appropriate water chemistry control. Furthermore, operational occurrences will not create water hammer in the surge line.

Based on the above, it is concluded that guillotine breaks in the pressurizer surge line should not be considered as a part of the structural design basis of the South Texas plant.

APPENDIX A

EQUILIBRIUM OF THE SECTION

APPENDIX A

The internal stress system at the crack plane has to be in equilibrium with the applied loading i.e. the hydrostatic pressure P, axial force F and the bending moment M_b. The angle β which identifies the point of stress inversion follows from the equilibrium of horizontal forces (See Figure A-1). This is

[ ] +a,c,e

Solving for β,

[ ] +a,c,e

The external bending moment at the instant of failure follows from the equilibrium of moments, which is most easily taken around the axis 1-1. Thus M_b can be determined from +a,c,e

[ ]

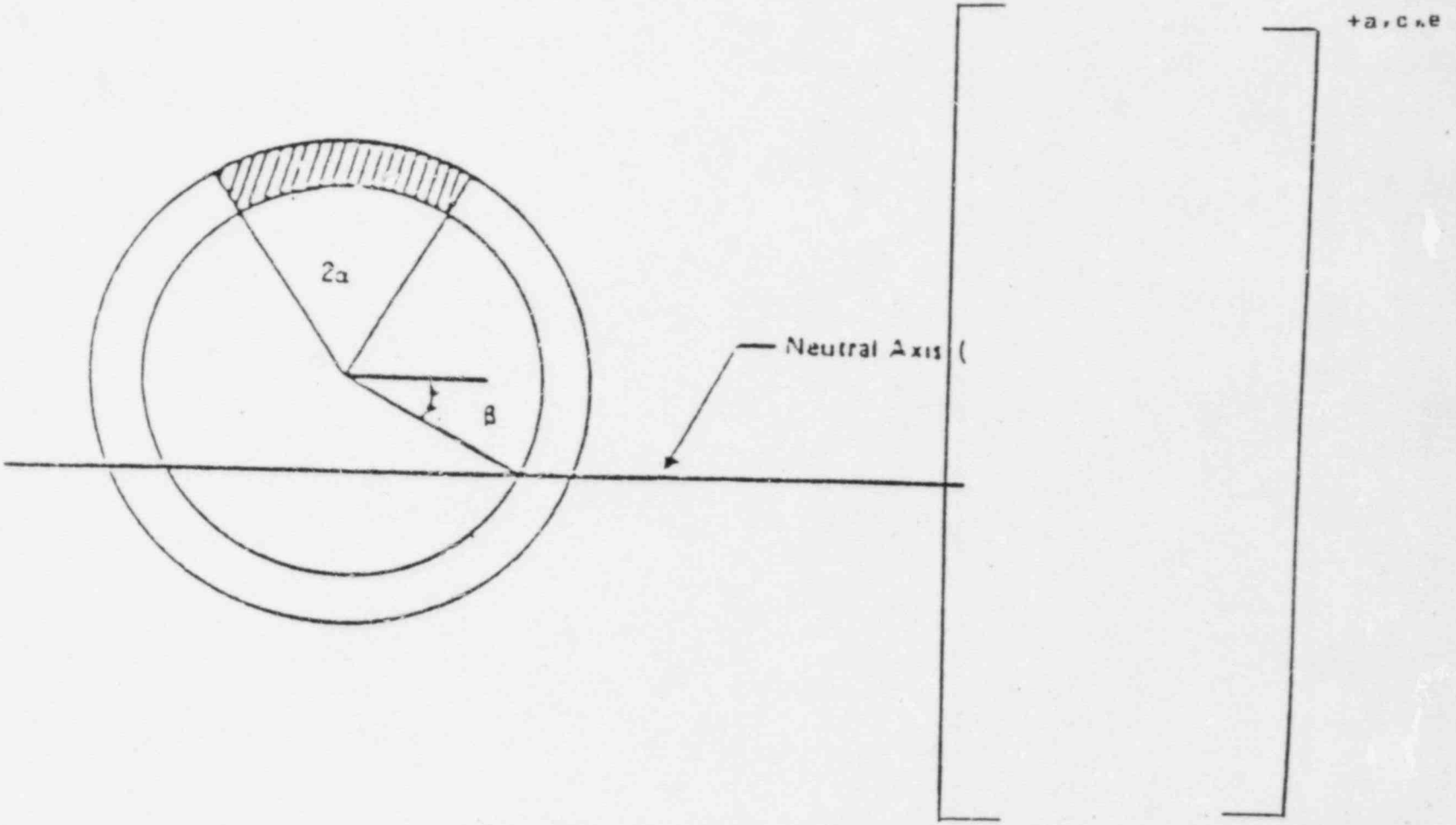

Figure A-1 Equilibrium of Horizontal Forces

APPENDIX B

NOMINAL STRESS STRAIN DIAGRAM

+a,c,e

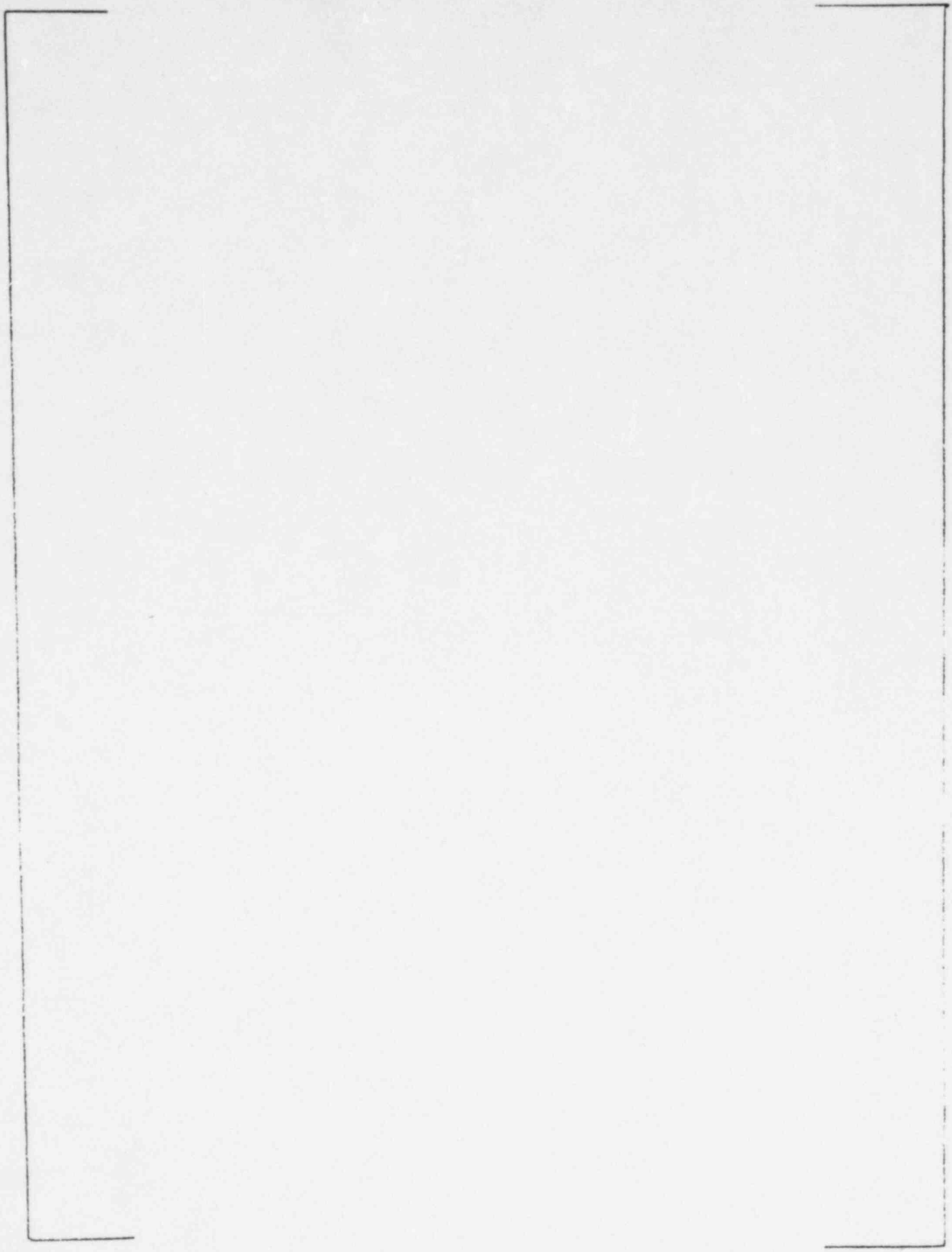

TABLE B-1

CONVERSIONS FROM TRUE STRESS STRAIN TO NOMINAL STRESS STRAIN

True Strain	Nominal Strain	True Stress	Nominal Stress

REFERENCES

[

] +a,c,e

B-2 "Engineering Materials - Their Mechanical Properties and Applications," Joseph Marin, Prentice-Hall, Inc., New York, 1953.

ADDITIONAL INFORMATION
SOUTH TEXAS SURGE LINE

The following additional information is provided in support of WCAPs 10489 and 10490 - "Technical Bases for Eliminating Pressurizer Surge Line Ruptures as the Structural Design Basis for South Texas Project". Item 1 clarifies aspects of the pipe loadings while Item 2 provides material toughness data for the piping and weldments and demonstrates that the leak-before-break criterion is met for the weldment in the critical location.

Item 1

The following paragraphs provide additional explanation of Section 5.2, "Loading the Model" in WCAP-10489 (proprietary class 2) and WCAP-10490 (non-proprietary).

The South Texas Project surge line is subjected to a pressure of [ ] a,c,e
The pressure causes an axial load of [ ] In addition, the pipe is a,c,e
subjected to other axial force of [
] Thus, the pipe is subjected to a a,c,e
total axial load of [ ] a,c,e

Since the [ ] an axial force does not re- a,c,e
sult by applying the pressure of [ ] surfaces. There- a,c,e
fore, to simulate the actual pipe loading an axial force of [
] has to be applied a,c,e
to the [ ] in the axial direction in addition to the pressure of [a,c,e
] applied to [ ] a,c,e

Item 2

In WCAPs 10489 and 10490 the weld connection between the [
] is identified as being the critical location for analysis. a,c,e
In the discussion below the maximum applied J values at the critical location are shown to be well below [ ] for the materials under consideration. Thus crack initiation is not [ ] the critical location and the leak-before-break criterion is met.

Figures 1 and 2 (taken from Reference 1 and annotated) present the typical high toughness of the 316 stainless steel forged pipe. Figure 1 gives the lowest J_{Ic} found. In the testing J values were obtained well in excess of of 12,000 in-lb/in^2. The highest value of applied J for this product form is found to be [ ] in-lb/in^2 in WCAP 10489 which is well below the minimum J_{Ic} reported in Reference 1 and given in Figure 1. Thus the flaw stability criterion is met when the piping base metal is considered. a,c,e

The fracture toughness of stainless steel welds has been found to range from about [ ] to over [ ] in recent studies. The weld J_{Ic} value of [ ] is representative of the lower toughness values available for stainless steel welds used in commercial fabrication and was obtained directly from Reference 2 and also published in Reference 3. Figure 3 presents the low toughness weld J-R curve results taken from Reference 2 and annotated. The higher results are found in Reference 4 and typical results are given in Figure 4 (taken from Reference 4 and annotated). For the lower toughness welds the yield strength is around 70 ksi (References 2 and 3). For the higher toughness welds, the minimum of the yield strengths is [ ] ksi (Reference 4). In the testing the J values obtained for the low toughness welds are seen to exceed [ ] in-lb/in^2 while for the high toughness welds, values exceeding [ ] in-lb/in^2 were obtained. a,c,e, a,c,e

In calculating the applied J for the welds, the elevated yield strength may be taken into account. The outer most fiber axial stress is [ ] which is well below the yield stress of [ ] ksi of the welds discussed in Reference 4. Therefore, the material is judged to remain in the elastic range. Thus, an applied K_I was calculated for the critical location using Reference 5 and converted to an applied J by the formula a,c,e a,c,e

$$J = \frac{K_I^2}{E}$$

The value of K_I obtained was [ ] which yielded a value of J of [ ] in-lb/in^2. This is well below the minimum J_{Ic} of [ ] in-lb/in^2. Hence, crack initiation will not occur and the flaw stability criterion is also met by the weld in the pipe. a,c,e a,c,e

REFERENCES

1. S. S. Palusamy and A. J. Hartman, Mechanistic Fracture Evaluation of Reactor Coolant Pipe Containing a Postulated Circumferential Through-Wall Crack, WCAP-9558, Rev. 2, Westinghouse Proprietary 2, Westinghouse Electric Corporation, May 1982.

2. Slama, G., et. al., Effect of Aging on Mechanical Properties of Austentic Stainless Steel Casting and Welds, presented at SMiRT Post Conference Seminar 6 - Assuring Structural Integrity of Steel Reactor Pressure Boundary Components, August 1983, Monterey, Calif.

3. Bamford, W. H., et. al., The Effects of Thermal Aging on the Structural Integrity of Cast Stainless Steel Piping for Westinghouse Nuclear Steam Supply Systems, WCAP-10465, Westinghouse Electric Corp., W Proprietary Class 2, Nov. 1983.

4. S. S. Palusamy, Tensile and Toughness Properties of Primary Piping Weld Metal for Use in Mechanistic Fracture Evaluations, WCAP-9787, Westinghouse Proprietary Class 2, Westinghouse Electric Corporation, May 1981.

5. Tada, H., "The Effects of Shell Corrections on Stress Intensity Factors and the Crack Opening Area of a Circumferential and a Longitudinal Through-Crack in a Pipe", Section II-1, NUREG/CR-3464, September 1983.

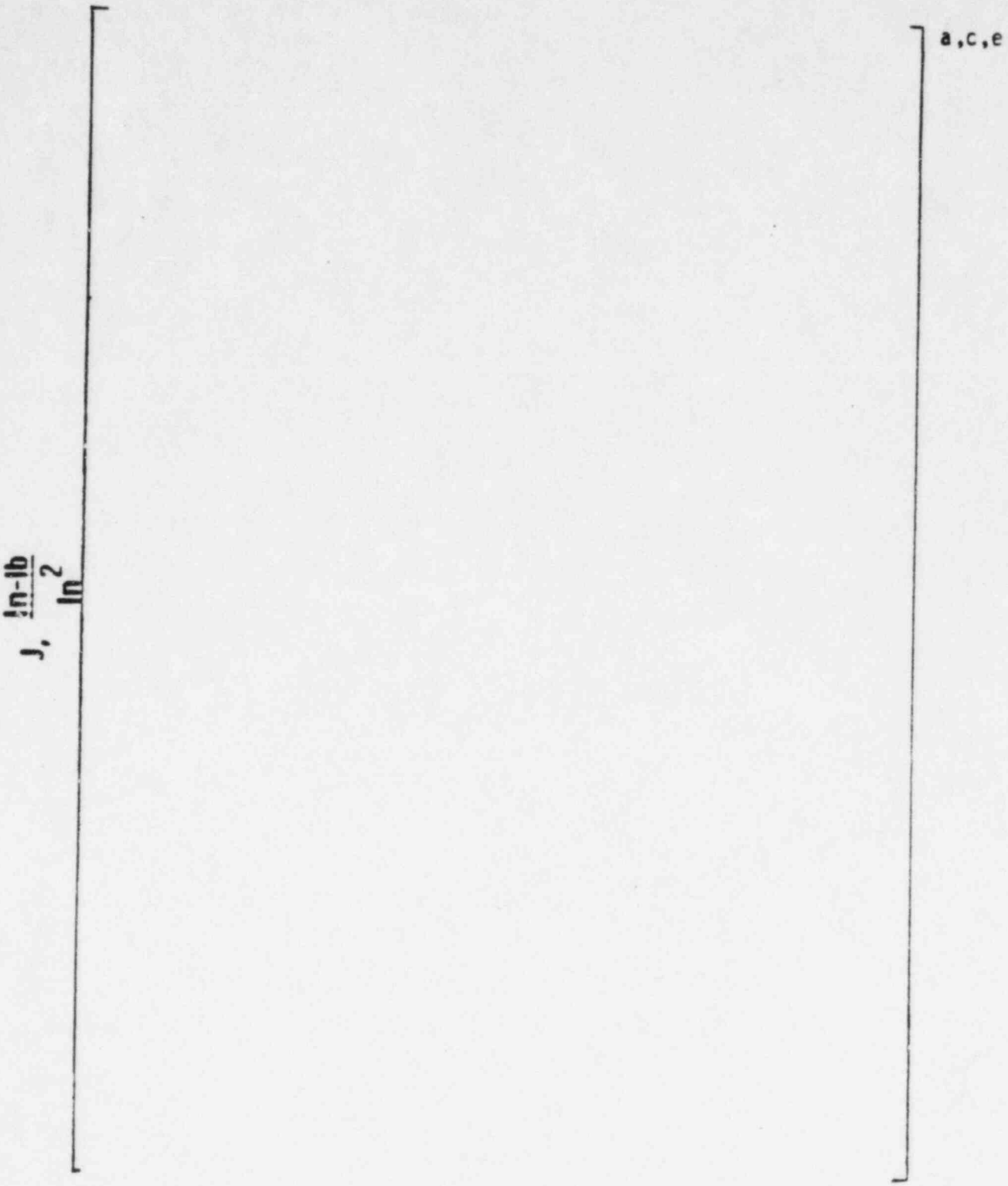

Figure 1 - J vs Δa for 316 stainless steel heat D8770 at 600°F, conventional loading

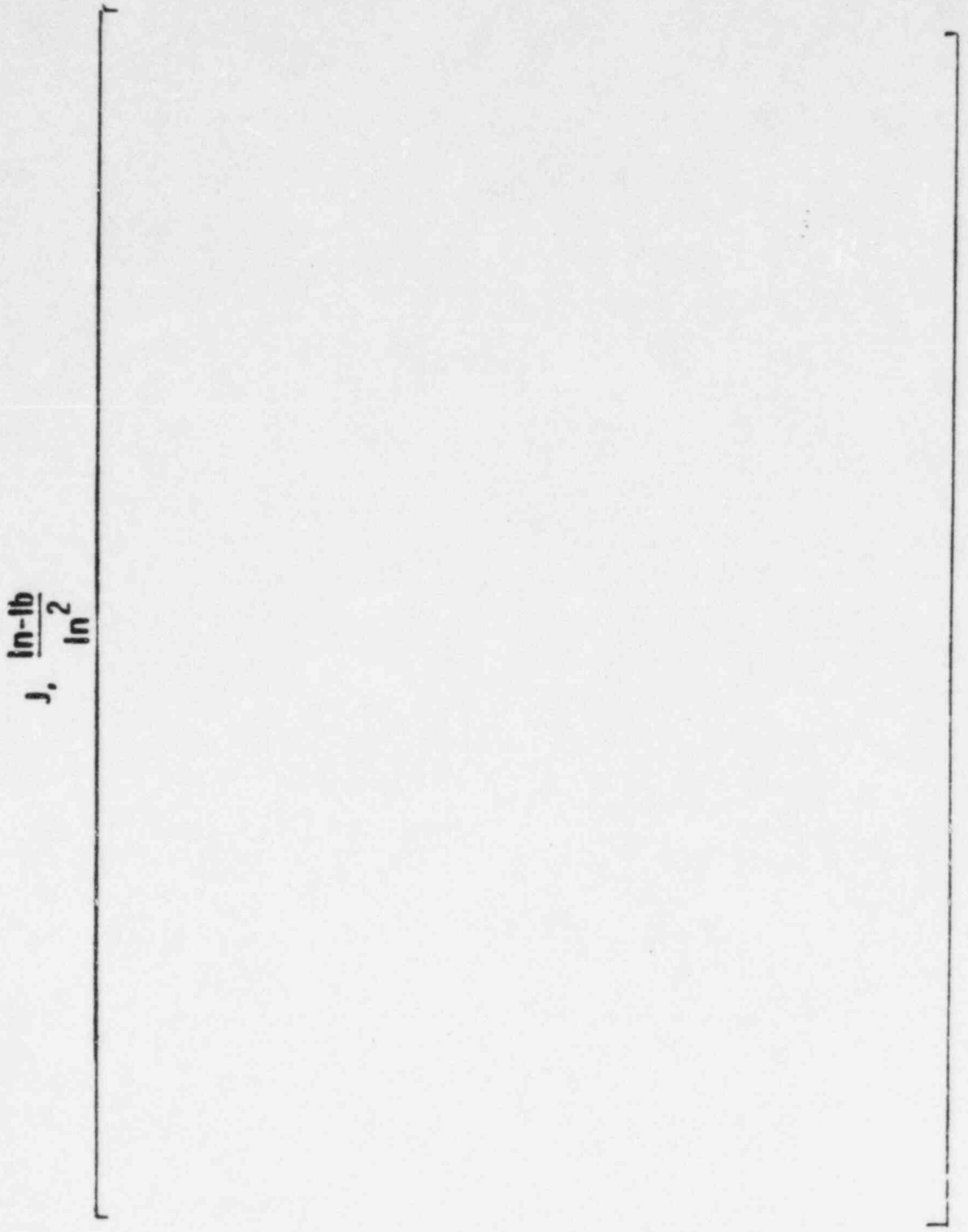

Figure 2 - J vs Δa for 316 stainless steel heat D8771 at 600°F, conventional loading rate

Figure 3 - [ ] a,c,e

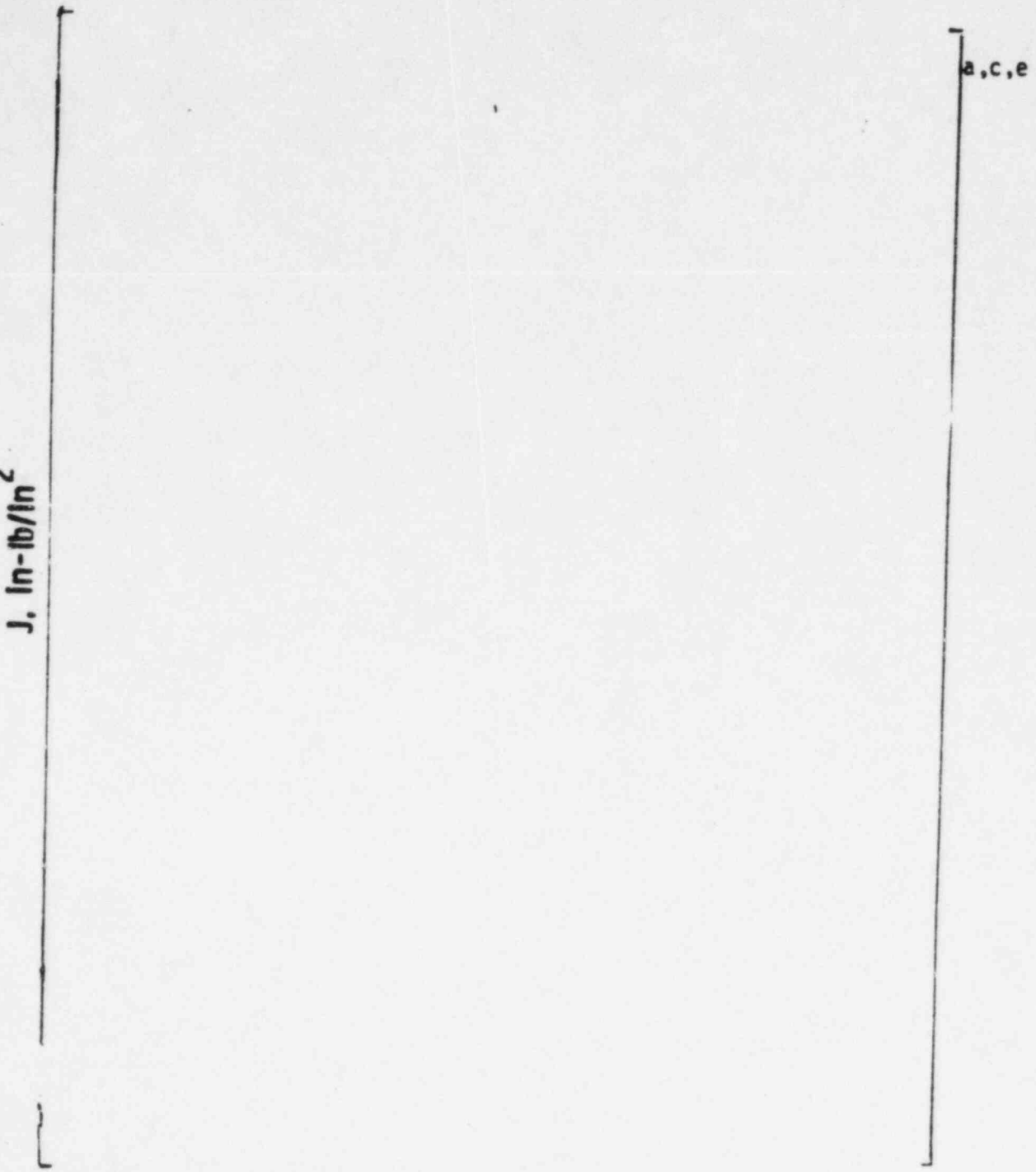

Figure 4 - J vs. Δa for the Stainless Steel Weldment SP4 at 600°F